JOURNAL OF GEOPHYSICAL RESEARCH, VOL. 98, NO. B9, PAGES 15,967–15,985, SEPTEMBER 10, 1993

Imaging Crustal Structure in Southwestern Washington With Small Magnetometer Arrays

GARY D. EGBERT

College of Oceanic and Atmospheric Sciences, Oregon State University, Corvallis

JOHN R. BOOKER

Geophysics Program AK-50, University of Washington, Seattle

We use data from a series of small (three to five stations) overlapping magnetovariational (MV) arrays to image variations of vertically integrated electrical conductivity in the crust of southwestern Washington. Two principal structures are revealed: a large north-south trending anomaly (the southern Washington Cascades Conductor (SWCC), which has been detected by several previous induction experiments), and a smaller anomaly which branches off of the SWCC just north of Mount St. Helens and trends westward beneath the Chehallis Basin. A weaker east-west trending anomaly is evident farther to the north beneath southern Puget Sound. The MV results concerning the SWCC are reasonably consistent with the model of Stanley et al. (1987), who interpret the anomaly as a suture zone of mid-late Eocene age, but the array data allows us to map the horizontal extent and complex three-dimensional character of the SWCC in greater detail. We suggest that the SWCC represents a section of the early Cenozoic subduction zone which is analogous to the present-day Olympic Peninsula. In the region west of the Cascades, the array data show that crustal conductivity is distinctly three dimensional, consisting of highly resistive blocks (crystalline rocks) separated (in the upper 5-10 km at least) by interconnected narrow regions of higher conductivity (sedimentary units). This pattern of conductivity variations is consistent with the inferred origin of the region as a seamount complex, which was subsequently broken into discrete blocks which have been thrust together during and after accretion to the North American continent. The distribution of anomalous electric currents and our model for crustal conductance are in striking agreement with a variety of other geophysical constraints, including gravity, magnetics, present crustal seismicity, and the pattern of recent volcanic vents. The St. Helens seismic zone (SHZ), which coincides with the western edge of the broad southern portion of the SWCC, is abruptly terminated in the north by the smaller east-west trending conductive zone. North of the SHZ near Mount Rainier, seismicity is concentrated in a narrow band coincident with the very narrow northern portion of the SWCC. In addition, volcanic vents are concentrated around the edges of the SWCC but are rare in the interior of the zone of high conductivity. The magnetometer array data thus suggest that present patterns of crustal deformation and volcanism are in part controlled by the complex tectonic history (and resulting crustal structure) of the region.

INTRODUCTION

The crust in western Washington is structurally complex, reflecting the tectonic history of the Pacific Northwest margin of North America (Figure 1). Since at least the earliest Tertiary, the geological development of the region has been dominated by the effects of plate convergence, although Basin and Range extension and most probably interactions with a mantle plume have also been important (see recent reviews by *Armentrout* [1987] and *Duncan and Kulm* [1989]). Ongoing seismicity and active volcanism in the Cascades magmatic arc attest to the continued convergence of the subducting Juan de Fuca and overriding North American plates. East of the Cascades in Washington, the basement consists of Mesozoic and Paleozoic rocks which were accreted to North America in the Mesozoic [*Cowan and Potter*, 1986]. West of the Cascades, the oldest rocks are the Paleocene to Eocene basalts of the Crescent, Siletz, and correlative formations [*Snavely et al.*, 1968; *Duncan*, 1982]. These basalts, which were erupted on an oceanic plate near North America and then accreted to the continent during late Eocene subduction, formed the basement on which a forearc basin subsequently accumulated [e.g., *Armentrout*, 1987]. The forearc basin rocks and the Eocene basalts (together called the Peripheral rocks by *Tabor and Cady* [1978]) form the Coast Range and the basins of the Puget Lowlands-Willamette trough.

Paper number 93JB00778.
0148-0227/93/93JB-00778$05.00

While the tectonic history and crustal structure of the region are understood in broad outline, there is much about this region that is in dispute. In particular, throughout most of Washington and Oregon the boundary between the Peripheral rocks and the older crust to the east has been completely covered by mid-late Tertiary and Quaternary volcanism in the Cascades. Direct observations of the location and nature of this suture are thus impossible. Similarly, the accumulation of forearc basin sedimentary and volcanic rocks obscures deeper structure in the Peripheral rocks. Geophysical methods for remote sensing of crustal structure are thus critically important to a further understanding of this complex region (see *Muffler* [1990] and references therein for a range of geophysical studies of this area). In this paper we use time variations of the geomagnetic field measured at an array of magnetometers to image large-scale variations of vertically integrated crustal conductivity in southwestern Washington.

Magnetovariational (MV) array data can be used to map anomalous magnetic fields induced in the Earth by time varying external sources. Such maps provide indirect estimates of the distribution of electric currents in the Earth and can be used to make inferences about lateral variations of conductivity, which in turn can be related to rock type [e.g., *Gough*, 1989]. We present a simple schematic model and overview of these ideas in Figure 2. To a large extent, the interpretation of MV data has been qualitative, with the existence of conductivity variations inferred from careful examination of geomagnetic event maps or from single-station horizontal to vertical field transfer functions (see *Gough et al.* [1989] for a recent example). However, much more can be gleaned from MV data when more sophisticated quantitative processing and inversion methods are employed [*Beamish and Banks*,

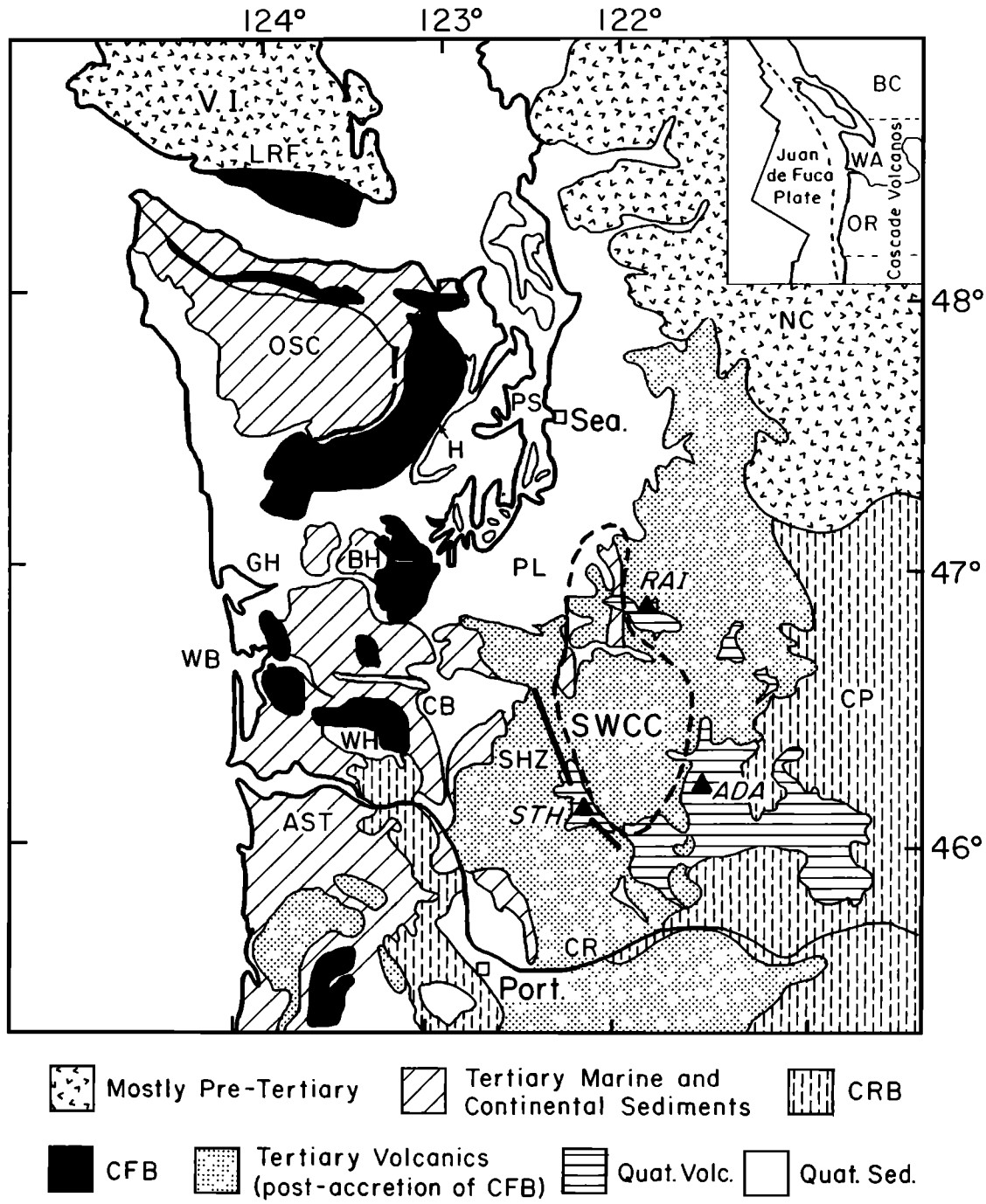

Fig. 1. Simplified geology map of western Washington. Inset gives location and regional tectonic setting (WA, Washington; OR, Oregon; BC, British Columbia; VI, Vancouver Island). Key features noted include: principal basins (CB, Chehallis Basin; PL, Puget Lowlands; AST, Astoria Basin; GH, Grays Harbor Basin), outcrops of the Crescent Formation Basalts (CFB, including BH, Black Hills, and WH, Willapa Hills), volcanic cover in the Cascades and to the east (RAI, Mount Rainier; STH, Mount St. Helens; ADA, Mount Adams; CP, Columbia Plateau, CRB, Columbia River Basalts), the Saint Helens Seismic Zone (SHZ), and the southern Washington Cascades Conductor (SWCC) mapped by *Stanley et al.* [1987]. Also, OSC, Olympic Subduction Complex; LRF, Leach River Fault; NC, North Cascades; CR, Columbia River; PS, Puget Sound; H, Hood Canal; Sea., Seattle; Port., Portland.

1983; *Banks and Beamish*, 1984; *Banks*, 1986; *Egbert and Booker*, 1989; *Egbert*, 1991]. Here we apply quantitative methods for MV array analysis to a series of small overlapping arrays run in southwestern Washington between 1980 and 1986. While our focus is on the final results and their significance for the geology and tectonics of this region, we also give, in the context of this illustrative case study, an overview and summary of the data processing and interpretation techniques used here.

BACKGROUND

Geology and Tectonic Setting

The study area in southwestern Washington occupies a section of the active Pacific Northwest margin of North America (Figures 1 and 3). The array covers an area which includes three Quaternary volcanos of the magmatic arc associated with oblique subduction of the Juan de Fuca plate (Figure 1): Mount St. Helens,

Mount Rainier, and Mount Adams. It is a seismically active area with a well-defined but abbreviated shallow dipping Benioff zone beneath the Puget Lowlands [*Taber and Smith*, 1985] and considerable crustal seismicity [*Ludwin et al.*, 1991], primarily in the Puget Lowlands and in a narrow belt trending north-northeast from Mount Saint Helens (the Saint Helens Seismic Zone, or SHZ [*Weaver and Smith* 1983; *Weaver et al.* 1987]).

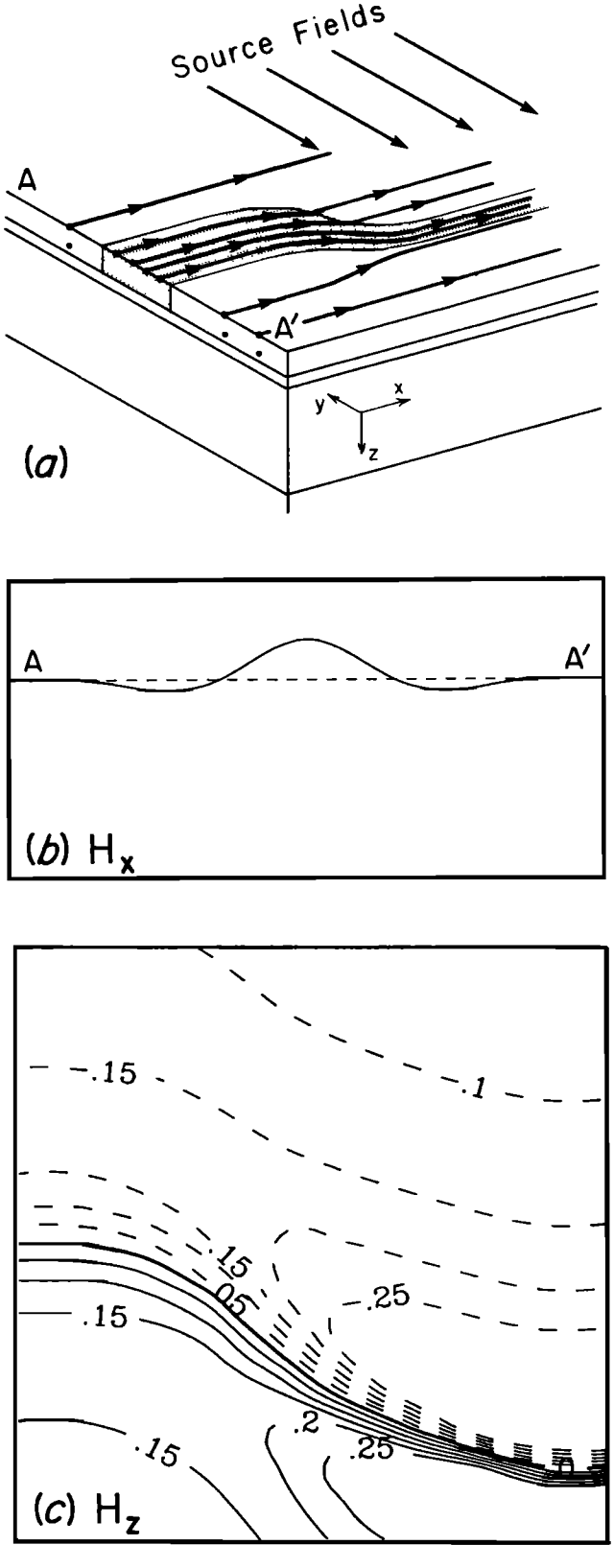

To the east and north of the MV array, the basement consists of Mesozoic and Paleozoic rock units. The western portion of the array is within the Coast Range province, which is underlain by the upper Paleocene to middle Eocene basalts of the Crescent, Siletz, and correlative formations. The thickness of these volcanics, which we refer to collectively as the Crescent Formation basalts, has been estimated at 3-7 km or greater by *Snavely et al.* [1968]. Petrologic and geochemical evidence imply that the Crescent basalts formed on oceanic crust as a chain of seamounts [*Snavely et al.*, 1968; *Duncan*, 1982]. Interbedding of basalts with distinctive continentally derived conglomerate implies that these islands were formed close to the margin of the North American continent [*Cady*, 1975]. After accretion, the Crescent basalts occupied the forearc of the convergent margin. From the middle Eocene to the middle Miocene, thick sequences of marine and nonmarine sediments and volcaniclastic rocks accumulated in the forearc basin [*Armentrout*, 1987]. Several pulses of volcanism also occurred during this time, producing the transitional oceanic Cowlitz volcanics (43-38 Ma), the magmatic arc Goble volcanics (38-29 Ma), and the Columbia River basalts (15 Ma), which flowed into the region from the east.

Paleomagnetic data require substantial (15°–80°) posteruption clockwise rotation of the Crescent basalts [*Wells*, 1990]. Three mechanisms of rotation have been proposed: (1) regional tectonic rotation of a rigid microplate during oblique collision with the North American continent, (2) rotation of the arc and forearc caused by intracontinental extension in the Basin and Range, and (3) dextral shear of the continental margin driven by the obliquely subducting Juan de Fuca plate [*Simpson and Cox*, 1977; *Magill et al.*, 1981; *Wells et al.*, 1984; *Wells*, 1990]. However, because overlying continental sedimentary and volcanic strata from the late Eocene are rotated nearly as much as the basement, it is probable that most of the rotation is postaccretion [*Wells et al.*, 1984]. In a summary overview, *Wells* [1990] concludes that rotation of the coast range of Oregon is probably due to a combination of the second and third mechanisms, while in southwestern Washington, rotation is dominated by dextral shear. In particular, in the Willapa Hills (the southwestern corner of the array, extending to the Pacific Ocean and the Columbia River) differential clockwise rotations of small structural blocks (~10 km) of 20–65° have been documented [*Wells and Coe*, 1985].

The Puget Lowlands-Willamette trough, a discontinuous set of

Fig. 2. Schematic overview of basic principles employed in mapping crustal conductivity variations with magnetometer arrays. (*a*) We emphasize a simple thin sheet model in which conductivity varies laterally in a surface layer. The shaded region is more conductive than the light background. Spatially uniform time varying magnetic fields induce electric currents in the Earth which are generally perpendicular to the inducing magnetic fields and tend to concentrate in the more conductive region. (*b*) Profile of the x component of the magnetic field H_x which would be observed along profile A-A'. The horizontal magnetic fields are a superposition of internal and external fields. Because of the concentration of currents, H_x is enhanced over the conductive zone (and slightly reduced to either side). (*c*) Plan view of vertical component H_z. The sign of H_z changes as the high conductivity zone is crossed. Since for quasi-uniform sources there is no external vertical component, H_z is due only to internal sources and thus clearly locates large-scale variations in conductivity. Note also that as the conductive zone narrows, the currents become more concentrated and are deflected and the amplitude of H_z increases. Variations of induced horizontal and vertical magnetic fields at the Earth's surface can thus be used to image lateral variations of electrical conductivity in the crust. As suggested by the simple model of Figure 2*a*, the method has relatively poor vertical resolution. Furthermore, without some independent knowledge of regional-scale deep conductivity variations, the absolute scale of conductance in the surface is only weakly constrained.

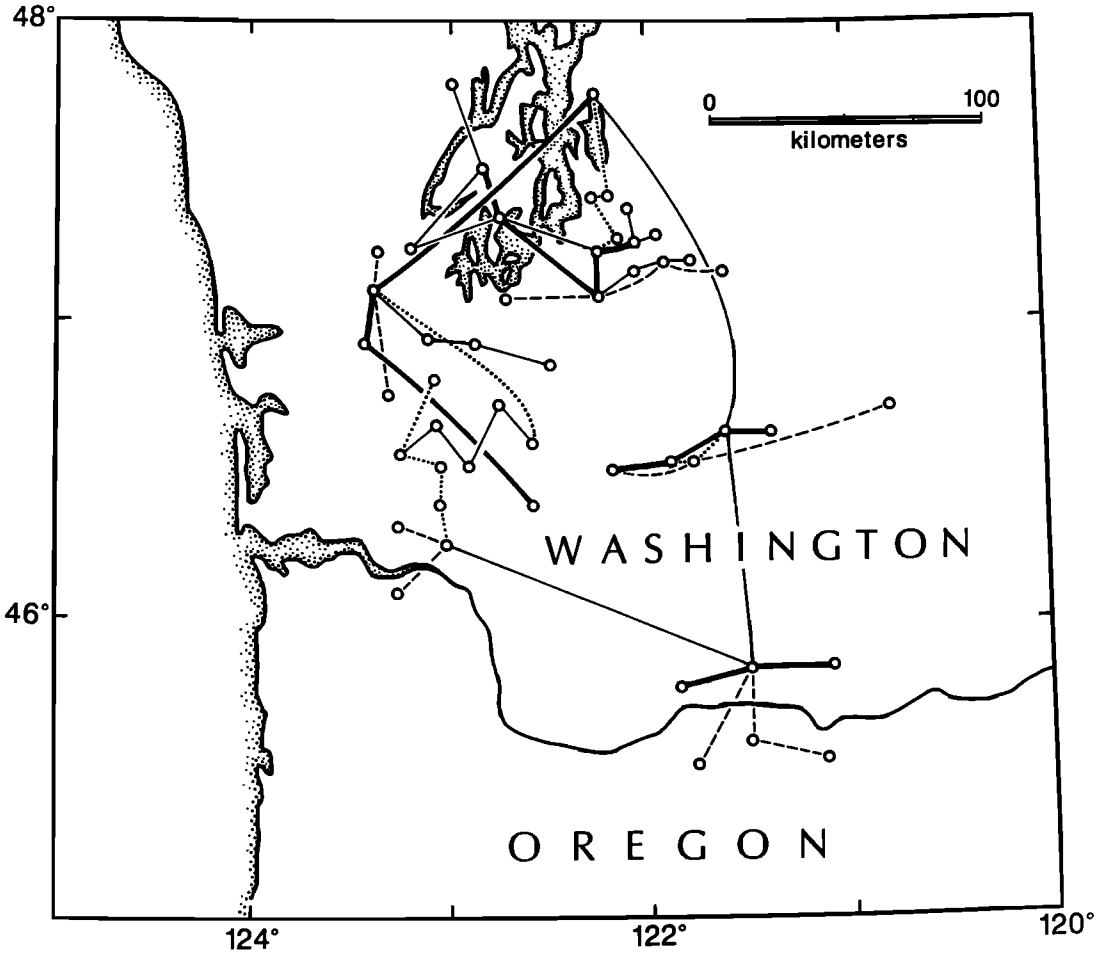

Fig. 3. Station locations and array connections for the 19 overlapping arrays in southwestern Washington State (containing a total of 49 stations) used for the analysis. All arrays are connected and can be combined into a single synthetic array.

basins extending from Puget Sound to southern Oregon, lies between the outcropping Crescent basalts of the Coast Range and the Cascades. Gravity and magnetic data suggest that a thick section (20-30 km) of dense mafic rocks, interpreted by *Finn* [1990] to be basalt and gabbro, underlies both the Coast Range and these basins, extending east to about the longitude of Mount St. Helens. This interpretation is supported by recent seismic refraction profiles to the south, which require a thick section of high-velocity crust underlying both the Coast Range and the Willamette Valley in central Oregon [*Trehu et al.*, 1992]. This suggests that the section of crust containing the Coast Range and the basins of the Puget Lowlands-Willamette trough should be considered as a unit. We will refer to this section of crust as the Coast Range block [*Finn*, 1990].

It is clear that there must be some sort of buried suture between this block and the older crust to the east [e.g., *Magill et al.*, 1981; *Duncan and Kulm*, 1989]. The northern boundary of the Coast Range block is the exposed Leach River fault in southern Vancouver Island (Figure 1). Here Crescent basalts are thrust under a subduction complex imaged by seismic reflection profiles to the north [*Clowes et al.*, 1987]. The southern boundary of the Coast Range block is exposed in southern Oregon in the Roseburg formation [*Magill et al.*, 1981]. Aeromagnetic, gravity [*Finn*, 1990], and seismic [*Snavely and Wagner*, 1982; *Trehu et al.*, 1992] data imply that the western boundary of the Coast Range block is offshore in Oregon and at the coast in Washington. However, the eastern boundary in Washington and north-central Oregon is obscure because of the essentially complete post-Eocene volcanic cover in the Cascades.

Previous Electromagnetic Studies in Southwestern Washington

Law et al. [1980] collected MV data at five sites in an east-west line which crosses the center of the array (Figure 3) and found evidence for a substantial conductivity anomaly beneath the Cascade range. They modeled this anomaly as a narrow north-south trending linear feature and concluded that the anomalous currents must be shallower than 25 km. The conductor was subsequently traced further to the north, almost to Seattle, by *Booker and Hensel* [1982], who suggested that the anomalous currents were due to channeling of currents from Puget Sound into a zone of high conductivity under the Cascades.

Further evidence for a substantial conductivity anomaly in this area was provided by *Stanley* [1984] and *Stanley et al.* [1987], who used magnetotelluric (MT) data from two roughly east-west profiles across the Cascades in southwestern Washington to construct two-dimensional models of crustal conductivity. *Stanley et al.* [1987] referred to this anomaly as the southern Washington Cascades Conductor (SWCC; see Figure 1). In these MT models the SWCC extends from near the surface to depths of 15 km or more and consists of very conductive (1-4 ohm m) rocks. *Stanley et al.* [1987] believe that the SWCC represents either an accretionary prism or forearc basin rocks which were accreted and subsequently compressed against the pre-Tertiary edge of the North

American continent in the mid-Eocene. Because shales hold water trapped in clays and zeolites and can remain highly conductive even at low porosities, *Stanley et al.* [1987, 1990] argue that the SWCC, which extends into the lower crust, where porosities should be low, is probably dominated by shale facies.

The SWCC is also clearly evident in the EMSLAB magnetometer array data [*Gough et al.*, 1989]. Data from this much larger scale array show that the SWCC is truncated in the north near Seattle and in the south near the Columbia river. However, the EMSLAB array data also detected a broader and deeper conductor continuing to the south under the high Cascades in Oregon. The EMSLAB MT data imply that this conductive zone is deeper than approximately 20 km [*Wannamaker et al.*, 1989]. *Gough et al.* [1989] suggest the possibility that this deeper conductor continues into Washington, where a shallow conductor is superimposed. In this view, the SWCC may represent a compound anomaly, which need not extend as a single unit through the crust.

Array Studies in Southwestern Washington

The data used for our analysis consist of three-component MV data collected at a total of 49 sites in a series of small arrays, each consisting of three to five simultaneous stations (Figure 3). All data were collected using EDA three-component fluxgate magnetometers [*Trigg et al.*, 1970] between 1980 and 1986. For the first eight of the arrays, data were collected at a 20-second sampling rate, with typical occupation times of approximately 4 to 5 days. For the 11 remaining arrays, data were sampled at an 8-second rate, and arrays ran for approximately 10 days each. Five of the arrays were occupied in their entirety more than once, so the total number of separate array experiments considered is 24. Some preliminary results from these experiments were reported by *Booker and Hensel* [1982], and *Egbert* [1991].

DATA PROCESSING: SMOOTH ESTIMATES OF INTERNAL ANOMALOUS FIELDS AND CRUSTAL CONDUCTANCE

In this section we summarize the MV array data processing methods applied to the southwestern Washington arrays. The raw data consist of a series of three-component magnetic field time series recorded in the overlapping arrays of Figure 3. Each time series is divided into a series of short segments, tapered, and Fourier transformed. The resulting Fourier coefficients form the basis for all further processing. The final result is a series of smooth maps of the period-dependent induced anomalous electric currents and an estimate of the vertically integrated crustal conductance.

Array Transfer Functions

The first step is to combine all of the frequency domain data into estimates of the total magnetic fields which would be observed at all stations in the combined array of Figure 3 if the external sources were perfectly uniform and linearly polarized in fixed directions (say, north-south and east-west). Simultaneous observations in an array can be used to estimate amplitudes and phases (or complex amplitudes) of all field components relative to the horizontal magnetic field components at a fixed reference site. This is accomplished in practice by using statistical transfer function methods, which combine all available data to improve signal-to-noise ratios and average out the effects of small-scale source variations [e.g., *Schmucker*, 1970; *Beamish*, 1977; *Egbert and Booker*, 1989]. If two or more separate arrays share a common station, the two arrays can be merged by using the common station as a reference [*Beamish and Banks*, 1983]. This process can be repeated for a series of overlapping arrays to yield estimates of relative amplitudes and phases between all stations in a large synthetic array [*Beamish and Banks*, 1983; *Egbert*, 1991]. For the results presented here, we have developed and used a multivariate generalization and refinement of the transfer function method which takes advantage of the simultaneous nature of array data [*Egbert and Booker*, 1989] and allows for optimal combination of overlapping arrays [*Egbert*, 1991]. A summary of these methods together with a detailed description of the initial processing of these arrays is given by *Egbert* [1991].

This first step results in estimates at a range of periods of the total (internal plus external) fields corresponding to induction by spatially uniform sources. In the absence of lateral conductivity variations, such sources induce laterally uniform currents in the Earth which flow at right angles to the external magnetic field. The resulting internal magnetic fields are in turn uniform and in phase with the inducing source fields [e.g., *Rokityanski*, 1982]. In this idealized case, the polarization and phase of the external source are thus uniquely determined from the observed total fields. Lateral conductivity variations result in (typically subtle) variations across the array in amplitude and phase of the total magnetic fields, making a precise determination of the external source characteristics problematic. In general, then, determination of the polarization and phase of the uniform external part of the observed fields requires some further assumptions. One approach to this problem [e.g., *Schmucker*, 1970] is to choose, on the basis of other geological and geophysical information, a fixed station as a normal reference. At this site the horizontal magnetic fields are assumed to be uncontaminated by lateral conductivity variations. The normal fields then implicitly define the polarization and phase of the external sources and can be subtracted from the total fields to yield estimates of the induced anomalous fields, which indicate geologic structure. We take a slightly different approach and assume that the fields averaged across the array are normal (i.e., correspond to a spatially averaged one-dimensional Earth [*Egbert and Booker*, 1989]). Note that with this definition of normal fields, the anomalous magnetic fields at all stations in the array must average zero for all polarizations.

The estimated anomalous horizontal magnetic fields for the combined southwestern Washington array are plotted for source fields linearly polarized north-south and east-west for a period of 1000 seconds in Figure 4. Note that the anomalous field vectors are complex (reflecting phase and amplitude variations), with imaginary parts generally much smaller than real parts. At most sites the anomalous fields are small relative to the normal fields (displayed in the upper right corners of the plots). Areas where the anomalous field vectors are negative (i.e., oppose the normal fields, as in the western part of the array in Figure 4*b*) represent relatively resistive regions with reduced current flow, while areas where the anomalous fields are positive (i.e., reinforce the normal fields, as in the area under the Cascades in Figure 4*b*) represent more conductive regions with enhanced current flow. Anomalous horizontal field vectors at angles to the normal (e.g., in much of Figure 4*a*) result from channeling and redistribution of electric currents by three-dimensional structures.

The exact magnitudes of the anomalous field estimates plotted in Figure 4 are somewhat sensitive to our definition of normal fields. However, because the normal fields are always taken to be spatially uniform, the pattern of variations in anomalous fields (and hence of relative conductivity variations) is well determined. Vertical magnetic fields are zero for induction by uniform sources in a one-dimensional Earth, so the total vertical component can be taken to be anomalous. The vertical components (real part only)

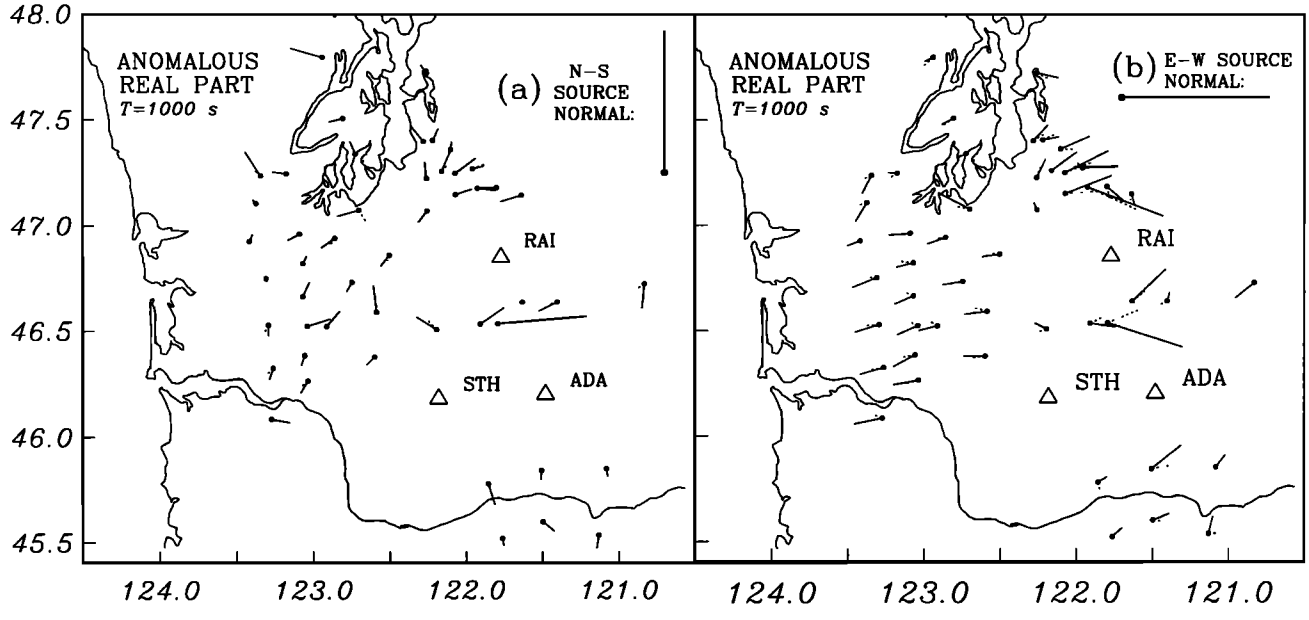

Fig. 4. Estimates of the complex anomalous horizontal magnetic fields which would be induced at stations in the combined array by sources with a period of 1000 seconds which are linearly polarized (*a*) north-south and (*b*) east-west. The total fields averaged over the array are assumed to be normal (i.e., representative of a spatially averaged one-dimensional Earth). The plotted anomalous fields represent the deviations from the normal vectors, which are given in the upper right corner of each plot. Solid vectors are real parts; dashed vectors are imaginary. Relatively conductive and resistive regions are characterized by areas where the anomalous field vectors respectively reinforce and oppose the normal fields. Anomalous field vectors at angles to the normal fields indicate channeling and redistribution of currents by three-dimensional structures.

for the southwestern Washington array are printed on a map of station locations, with informal contours to guide the eye, in Figure 5.

Figures 4 and 5 exhibit three principal features. First, the vertical component corresponding to an east-west source polarization is positive over much of the array, increasing to rather large values as the coast is approached in the west (Figure 5*b*). This is the well-known "coast effect" [e.g., *Parkinson*, 1962; *Everett and Hyndman*, 1967] resulting from a concentration of north-south electric currents flowing in the ocean and conducting sediments of the accretionary wedge at the continental margin [*Weaver*, 1962]. Superposed on the coast effect are vertical anomalous fields which reverse sign along a north-south trending line which passes through the SWCC (Fig. 5*b*). Evidence of the SWCC is also seen in the anomalous horizontal fields of Figure 4*b*, which are enhanced (at all available stations) in a belt passing through the three Cascade volcanos from the Columbia river to Puget Sound and in both the vertical and horizontal anomalous field plots corresponding to north-south source polarizations (Figures 4*a* and 5*a*). Finally, an anomaly extends west from the SWCC just north of Mount St. Helens along the northern edge of the Chehallis Basin. This feature is seen for north-south source polarizations as an enhancement of the horizontal fields (Figure 4*a*) and a sign reversal in the vertical fields (Figure 5*a*). We refer to this feature as the Chehallis Basin Conductor, or CBC for short. Using the right-hand rule for the Biot-Savart law, it is readily verified that the horizontal and vertical components of the anomalous fields over the SWCC and CBC are both consistent with electric currents inside the Earth.

Figures 5 and 6 represent only a small sample of the anomalous field plots which result from the initial data processing. For each frequency band there are real and imaginary and horizontal and vertical field plots for each of two polarizations. Using a 25% bandwidth (≈ 9 bands per decade) in the frequency domain, estimates have been obtained for the southwestern Washington synthetic array in 20 bands at periods from 60 to 10,000 s. The full set of 160 plots represents a complete estimate of the response of the Earth (in this period range at the available sites in the region) to uniform external magnetic field sources. In general, these response estimates vary smoothly with period. For subsequent discussion we will focus on results from four representative bands evenly spaced in log period: $T = 100$ s, $T = 300$ s, $T = 1000$ s, and $T = 3000$ s.

Spline Smoothing of Internal Fields

Figures 4 and 5 are estimates at a discrete set of points of the anomalous magnetic fields. The next processing step involves smoothing and interpolation onto a regular grid, subject to the constraint that the interpolated anomalous magnetic fields be physically consistent with sources of strictly internal origin. To do this, we treat interpolation as a linear inverse problem [*Egbert*, 1989]. The constraints are imposed by requiring that the magnetic fields be the gradient of a scalar potential with all sources below the surface. We then seek the smoothest internal potential which is consistent (within the estimation errors) with the synthetic array response. This approach is very similar to the method of harmonic splines developed by *Shure et al.* [1982] and *Parker and Shure* [1982] to find smooth magnetic fields at the core mantle boundary from observations at the Earth's surface. However, the rectangular geometry appropriate for regional arrays and uncertainty about the depth of the sources result in some mathematical complications [*Egbert*, 1989]. The key results needed to solve this problem are proved by *Meingut* [1979], who developed a natural generalization of cubic splines for interpolation of data in a multidimensional setting, and by *Wahba and Wendelberger* [1980], who consider the application of these "multivariate splines" to more general inverse problems.

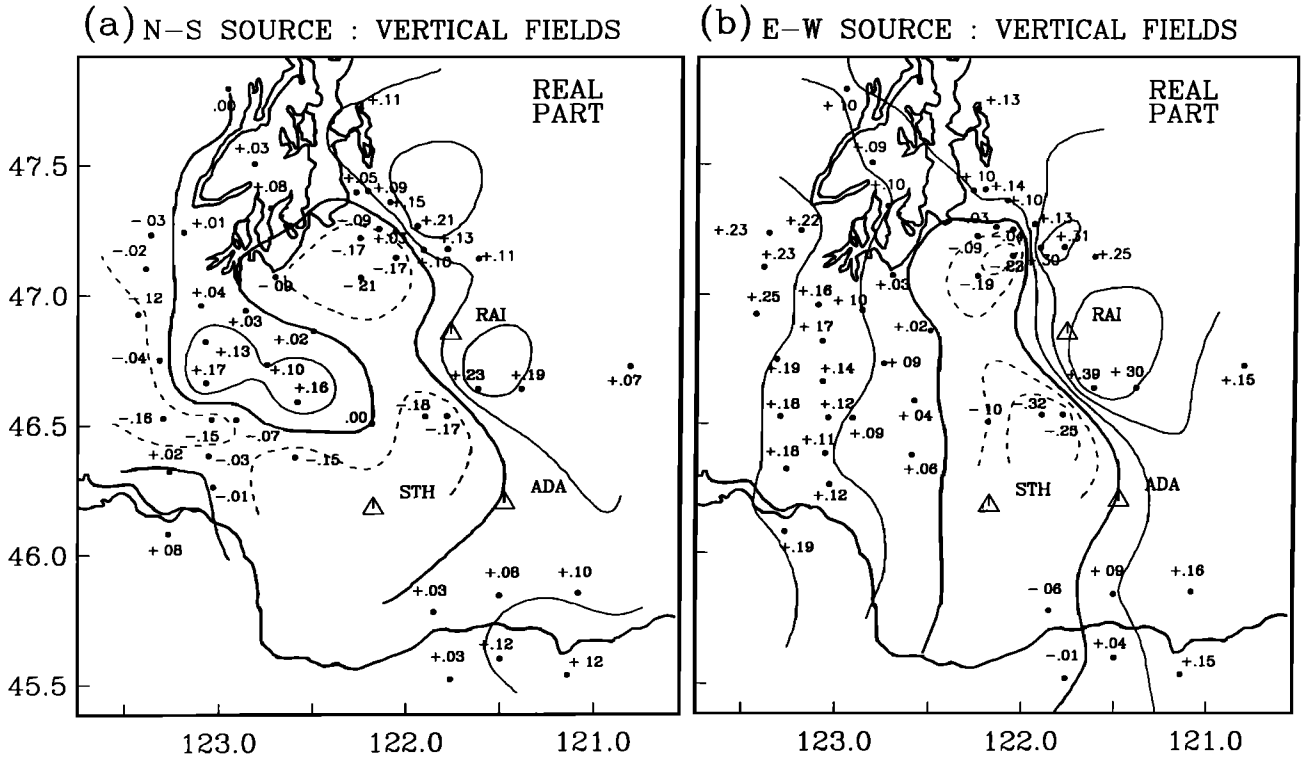

Fig. 5. Estimates of real parts of anomalous vertical fields which would be induced at stations in the combined array by sources with a period of 1000 seconds which are linearly polarized (*a*) north-south and (*b*) east-west. Positive values of the vertical component correspond to magnetic field vectors which point down into the Earth. Three substantial anomalous features are evident here: the large positive vertical field in the western part of the array in Figure 5*b* is the coast effect, resulting from electric current flowing in the conductive ocean and sediments of the accretionary wedge. The north trending reversal in sign under the Cascades (in Figures 5*a* and 5*b*; note also the enhancement of horizontal components in this area in Figures 4*a* and 4*b*) coincides with the SWCC; finally, a smaller east-west conductive zone is marked by the east-west trending sign reversal which branches off of the SWCC to the west just north of Mount St. Helens. This anomaly is also visible in Figure 4*a*.

Plots of the smoothing spline estimates of the anomalous horizontal and vertical magnetic fields are given in Figures 6 and 7 for a period of 1000 s. Note that because the interpolation procedure allows for the actual estimated errors at each site, these smooth fields do not exactly interpolate the discrete response estimates of Figures 4 and 5.

The processing methods reviewed so far can be thought of as a generalization and refinement of the vertical field hypothetical event map [*Bailey et al.*, 1974]. However, instead of using only single-station vertical field transfer functions, all possible interstation and intercomponent transfer functions are incorporated along with the physical constraint that the source for the anomalous fields be internal. Because horizontal components of the anomalous fields are sensitive to structure immediately below the observation point while vertical components are sensitive to structure off to the side, using anomalous horizontal fields and the a priori physical constraints effectively increases horizontal spatial resolution (e.g., compare the vertical field contours in Figures 5 and 7).

There are still some significant holes in our station coverage, particularly near each of the three Cascade volcanos and on the eastern edge of the array. Because our procedure finds the smoothest anomalous fields consistent with the available data, these unsampled regions are interpolated across smoothly without including unnecessary details. Of course, with additional sites, smaller-scale features would undoubtedly be evident. Note, however, that the unsmoothed anomalous fields (Figures 4 and 5) do generally vary slowly between adjacent stations. This gives us some confidence that the large-scale pattern of smooth anomalous fields plotted in Figures 6 and 7 are not seriously affected by aliasing. In particular, all of the lines which cross the SWCC between Puget Sound and the Columbia River show a similar pattern of sign reversal in the vertical component and enhancement of the horizontal component. Given the strong north-south spatial coherence of the available anomalous fields, it is virtually certain that additional east-west transects across the Cascades would reveal a grossly similar pattern of anomalous fields.

Equivalent Sheet Currents

Using the Biot-Savart law, horizontal magnetic fields of internal origin can be transformed to an equivalent surface current sheet (i.e., a thin sheet of current below the observer which would reproduce the fields), by rescaling and rotating the magnetic fields 90° counterclockwise [*Banks*, 1979] (see also the appendix). Applying this transformation to the anomalous magnetic fields of Figure 7 clearly displays the anomalous current flow discussed above (Figure 8).

Although the induced anomalous currents are periodic, with the phase and polarization varying across the array, it will often be useful to refer to the "direction" of equivalent current flow. For this purpose it is convenient to treat real and imaginary parts as separate vectors. Note that the real current sheets are in phase with the reference external magnetic fields. The imaginary parts of the current vectors represent magnetic fields which lead the reference fields by 90°. We refer to the real and imaginary parts as the in-phase and quadrature currents, respectively.

The currents of Figure 8 tend to flow in vortices which close on

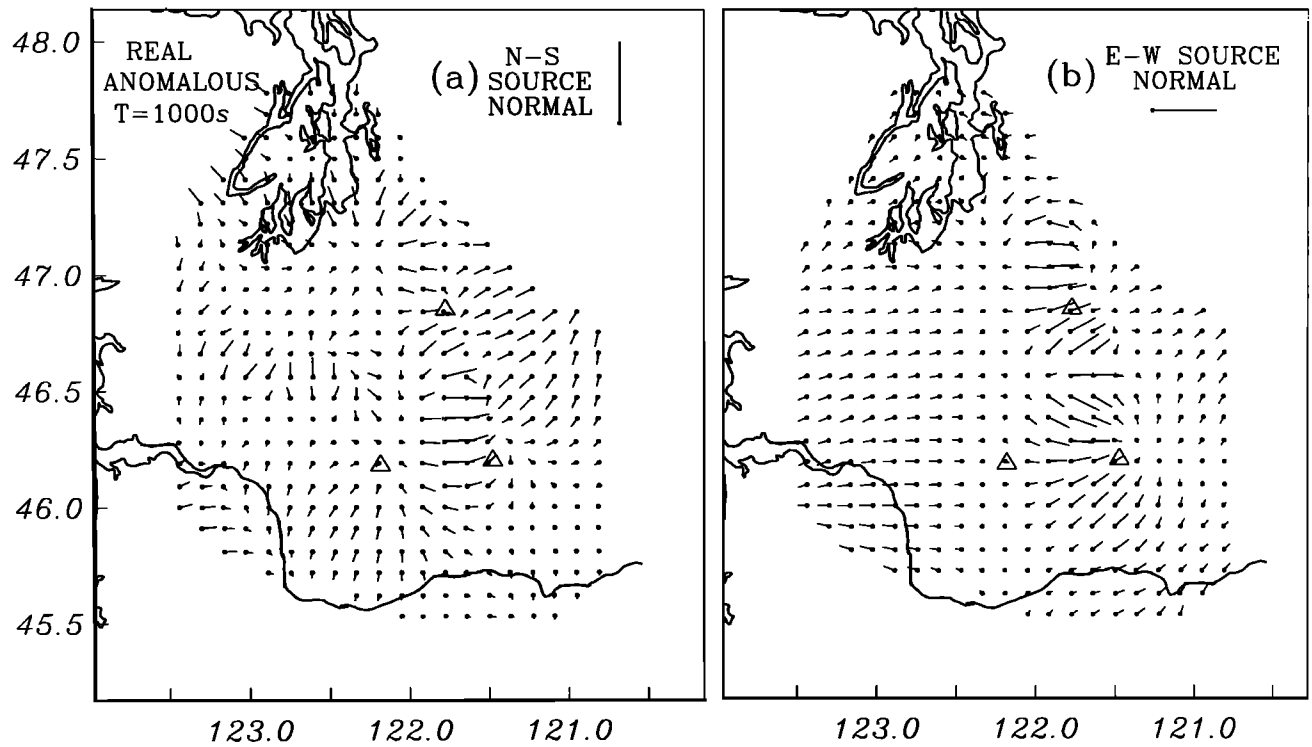

Fig. 6. Smoothing spline interpolation of three-component magnetic field vectors. The figure gives the real part of the horizontal components of the smoothest magnetic fields of internal origin that are consistent (within the estimation errors) with the estimated anomalous fields of Figures 4 and 5. (*a*) north-south source polarization. (*b*) east-west source polarization.

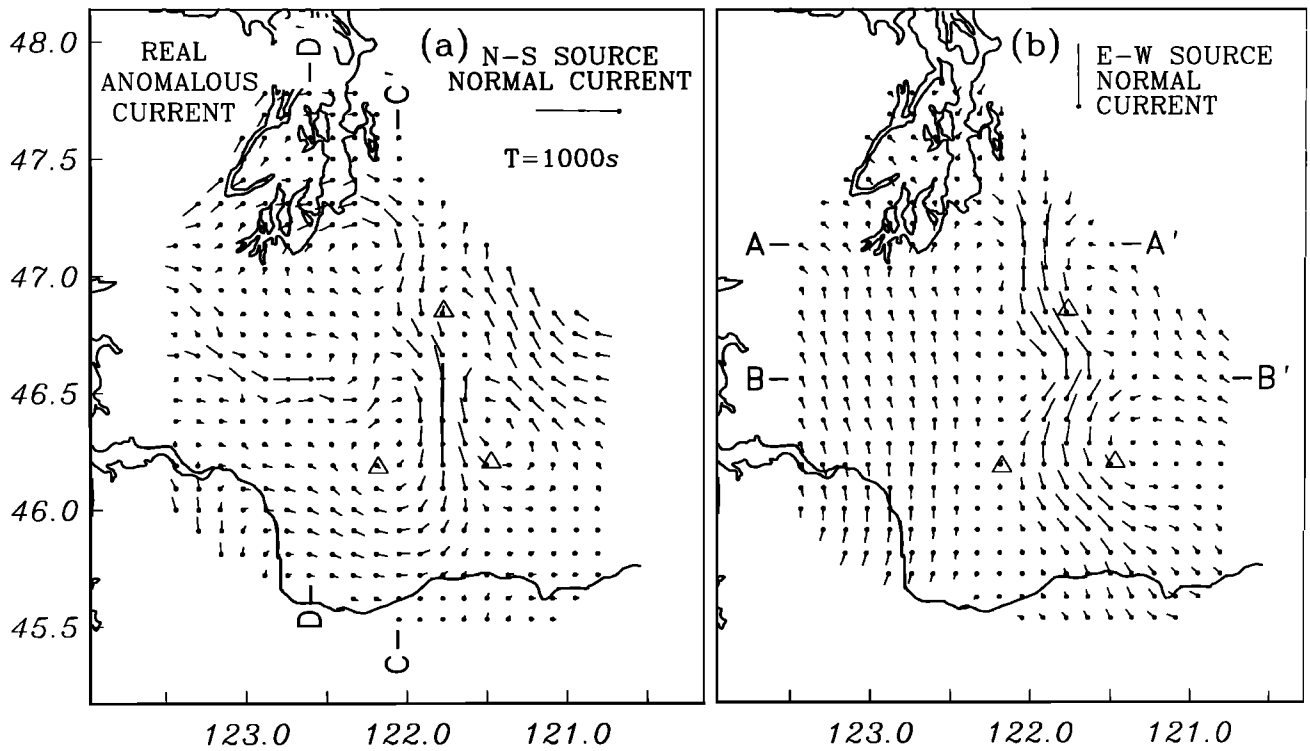

Fig. 7. As in Figure 6 but vertical component for (*a*) north-south source polarization and (*b*) east-west source polarization.

themselves, and in places they oppose the "normal" current. This is a result of the way we have defined anomalous fields, which must average to zero. Relatively conductive areas, where current flow is enhanced (with anomalous currents reinforcing the normal), must be balanced by relatively resistive areas, where current flow is reduced (with anomalous currents opposing the normal). In the simple schematic model of Figure 2 a laterally heterogeneous surface layer overlies a one-dimensional deep section. The total current at period T which flows in the surface layer can be written

$$\mathbf{I}(\mathbf{x}, T) = \mathbf{I}_0(T) + \delta\mathbf{I}(\mathbf{x}, T), \quad (1)$$

where $\delta\mathbf{I}(\mathbf{x}, T)$ represents the anomalous currents (which average to zero) and $\mathbf{I}_0(T)$ represents the normal current flowing in the

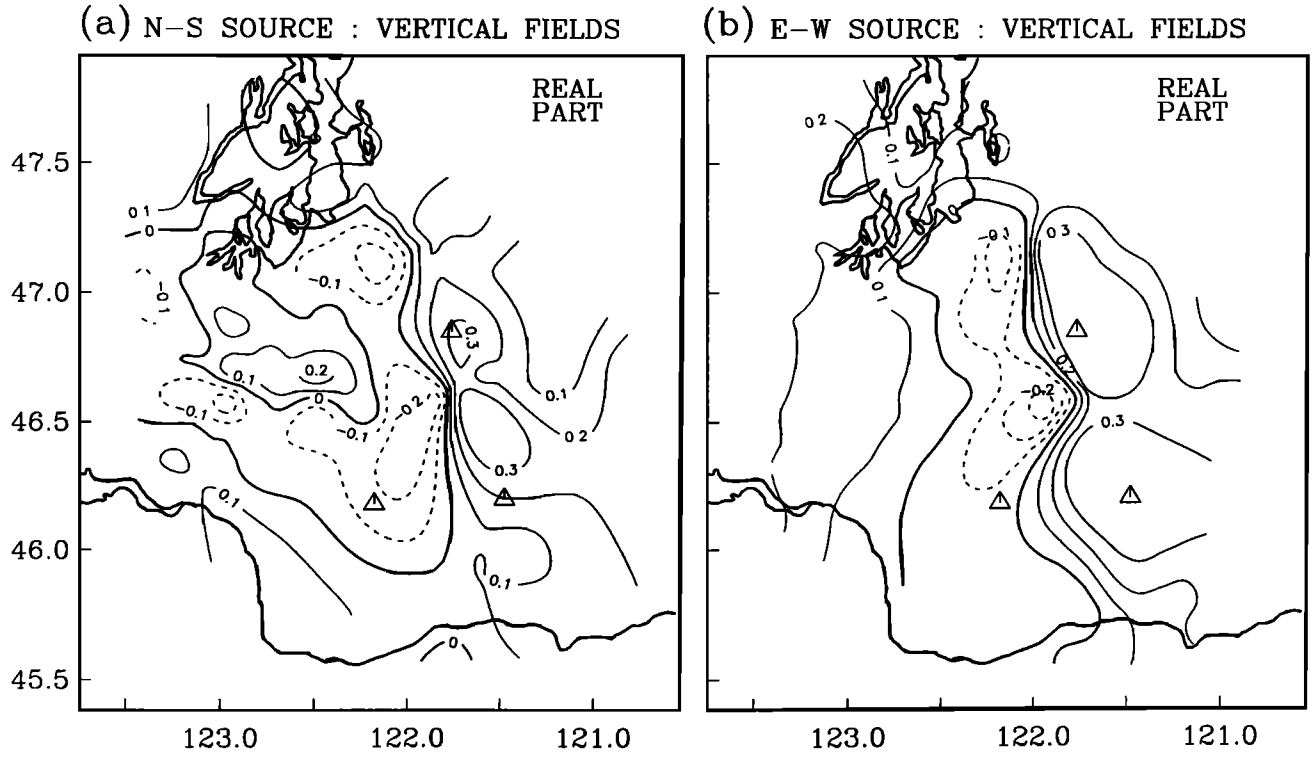

Fig. 8. Real parts of anomalous equivalent sheet currents for two source polarizations. The vectors in these plots are obtained by rotating the anomalous magnetic field vectors of Figure 6 90° counterclockwise. The vectors are tangent to streamlines of an equivalent surface sheet current which would reproduce the smooth magnetic fields. For Figure 8*a* the normal current flow is from east to west, while for Figure 8*b* the normal current flow is from south to north. Because the spatial average of the anomalous magnetic fields (and hence of the current sheet) is zero, the anomalous currents tend to flow in vortices which close on themselves. A-A' through D-D' mark locations of profiles plotted in Figures 11 and 12.

thin sheet. With the MV array data we can readily estimate $\delta\mathbf{I}$. Unfortunately, while consistency of the total currents with the physics of electromagnetic induction (and the simple considerations discussed below) provide some information about $\mathbf{I}_0$, the absolute magnitude of this quantity is poorly constrained by the MV data (see the appendix).

However, estimates of $\mathbf{I}$ are highly desirable. As discussed below, total currents but not anomalous currents can be easily inverted for crustal conductance. Furthermore, the total current is relatively large in conductors and small in resistors, so lateral conductivity contrasts (and the manner in which currents are redirected and channeled in complex three-dimensional structures) are more clearly illuminated in plots of $\mathbf{I}$. These advantages are illustrated in Figures 9 and 10, where we plot rough estimates of total crustal currents (compare to Figure 8).

In the long-period limit, where induction in the surface sheet can be ignored and galvanic redistribution of the currents dominates, the period dependence of the currents in the thin sheet model can be separated from the spatial dependence [e.g., *Le Mouel and Menvielle*, 1982]

$$\mathbf{I}_0(T) + \delta\mathbf{I}(\mathbf{x},T) \simeq I_0(T)[\mathbf{i}_0 + \delta\mathbf{i}(\mathbf{x})]. \quad (2)$$

Here, $\mathbf{i} + \delta\mathbf{i}(\mathbf{x})$ is a real vector field (independent of period, divided as in (1) into constant normal and spatially varying anomalous parts) and I_0 is a complex scalar. From (2) we see that $I_0(T)$ is determined, (at sufficiently long periods) up to a single real scalar by our estimates of $\delta\mathbf{I}$. Thus fixing Re $\mathbf{I}_0$ for a single period determines both the in-phase and quadrature total currents for all sufficiently long periods. We have used this idea to estimate the currents in Figures 9 and 10 by choosing (somewhat subjectively) Re $\mathbf{I}_0$(1000 s) for each polarization and then scaling $\mathbf{I}_0(T)$ (separately for the real and imaginary parts) by the relative root mean square (RMS) of (the real and imaginary parts of) $\delta\mathbf{I}$ for each period T.

Current vectors in each of these plots are also scaled by the anomalous current RMS so that the typical lengths of the displayed vectors is constant. The RMSs of the total sheet currents (in-phase and quadrature separately) are displayed in the upper left corner of each plot. This display of the currents allows for an approximate separation of amplitude and phase variations (which we expect to be dominated by $\mathbf{I}_0$) from variations in the geometry of the current sheet. Note that except for the quadrature currents at the shortest periods, the geometry of the currents varies little. This is consistent with (2), giving us some confidence that our thin sheet model is approximately valid. A more detailed discussion of these plots is deferred to the results section.

Simple Inversions for Conductance

In the model of Figure 2, a thin surface sheet of variable conductance (conductivity times thickness)

$$S(x, y) = S_0 + \delta S(x, y) \quad (3)$$

overlies a layered one-dimensional Earth. For the final processing step we adopt this simple model for the crust of southwestern Washington and invert the sheet currents for crustal conductance S. This model ignores any vertical structure in the upper inhomogeneous layer and further assumes that the layer is very thin compared to the penetration depth of the electromagnetic fields. The thin sheet model is thus most reasonable at long periods, where penetration depths are greatest and vertical resolution of the MV data is very poor. In the simplest sort of thin sheet model, the upper inhomogeneous layer is separated from deeper layers by a layer of infinite resistance which prevents vertical flow of currents [*Price*, 1949]. For this model a simple direct (almost linear)

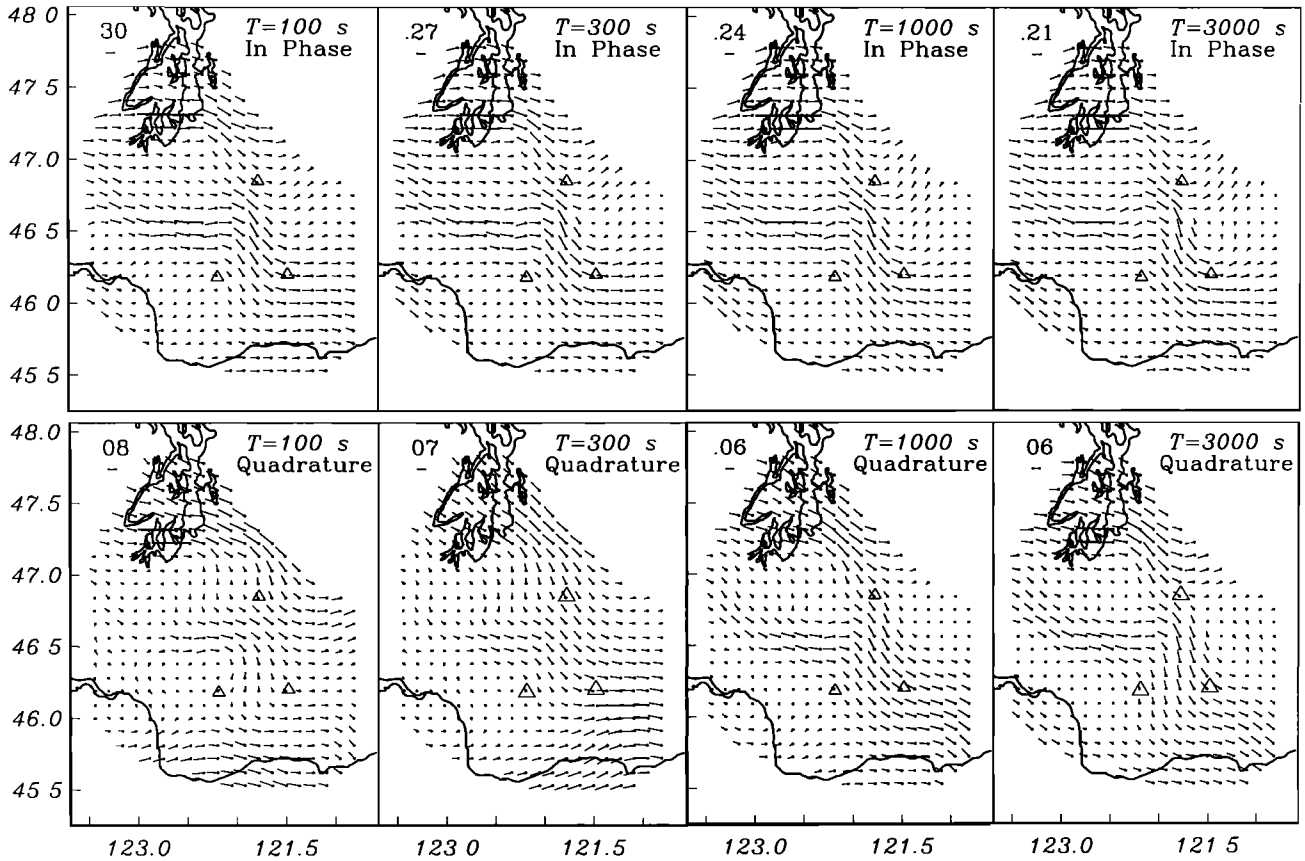

Fig. 9. In phase and quadrature parts of estimated total surface sheet current induced by north-south source polarization for four periods. The scales for current vectors (given in the upper left corner of each plot) are proportional to the relative RMS amplitude of the anomalous currents averaged over the array. The total sheet current is formed by adding an estimate of the constant "normal" current $\mathbf{I}_0$ to the anomalous currents. For the in phase part at $T = 3000$ s $\mathbf{I}_0 = .03\hat{\mathbf{x}} - .18\hat{\mathbf{y}}$, where $\hat{\mathbf{x}}$ and $\hat{\mathbf{y}}$ are unit vectors pointing to the north and east respectively. For the shorter periods this vector is rescaled according to the relative RMS of the anomalous fields. The normal quadrature currents are chosen similarly, with $\mathbf{I}_0 = .02\hat{\mathbf{x}} - .04\hat{\mathbf{y}}$ at $T = 3000$ s. The locations of the three Cascade stratovolcanos (Mount Rainier, Mount St. Helens, and Mount Adams) are given by the large triangles. All of the plots, except those for the short period quadrature currents, are very similar. Although normal current flows from east to west, substantial current is channeled to the north in the SWCC. In the western part of the array, current flows west in two conductive channels, one just north of Mount St. Helens and the other at the northern end of the array.

inversion of sheet currents for crustal conductance is possible [*Berdichevsky and Zhdanov*, 1984]. We outline a practical implementation of this inversion in the appendix. This approach is simplistic but not completely unreasonable. Most of the anomalous structure evident in the current sheet plots (Figures 9 and 10) originates in the crust (the anomalies are tens of kilometers wide and are nearly independent of period), and highly resistive layers are typically present in the crust and upper mantle.

Application of the simple thin sheet inversion outlined in the appendix to long-period ($T = 1000$ s and $T = 3000$ s) anomalous fields from the synthetic array yields the model of crustal conductance shown in Plate 1. With this simple approach to inversion, two parameters which are not directly constrained by the MV data must be independently estimated: the normal current in the thin sheet $\mathbf{I}_0$ and the normal conductivity S_0. In fact, the absolute scale of crustal conductance in the model of Plate 1 is essentially determined by the choice of S_0 (here taken to be 100 S, equivalent to a 20-km-thick 200-ohm m layer). Further uncertainty in the relative variations of crustal conductance results from uncertainty concerning $\mathbf{I}_0$. Experiments with a range of values of $\mathbf{I}_0$ indicate, however, that the geometry of the conductivity variations is very well constrained and that the relative amplitudes of the variations (i.e., the ratio of highest to lowest conductance) are constrained within a factor of roughly 3.

Note that full nonlinear inversions of the combined array response, based on either more general thin sheet [e.g., *Vasseur and Weidelt*, 1977; *Fainberg et al.*, 1990] or fully three-dimensional models, would substantially reduce this scale ambiguity, particularly if constraints on known large-scale structure (e.g., ocean bathymetry and conductivity) were incorporated. These more complicated inversion methods represent an important refinement of MV interpretation methods which we are currently pursuing.

RESULTS

The final results of the processing are contained in Figures 9 and 10 and Plate 1. The equivalent current sheets (Figures 9 and 10) are estimates of the total current flowing in a thin surface layer of laterally varying conductance (Figure 2). Plate 1 gives an estimate of the conductance of this surface layer. The currents in Figures 9 and 10 have widths of 10-40 km (see also Figures 6 and 8). The true anomalous current distribution is almost certainly rougher than these smooth estimates. These short-length scales imply that the anomalous currents flow within at most a few tens of kilometers of the surface. The vertical distribution of conductivity within this near surface region is not resolved by the thin sheet model of Plate 1. However, we can gain some qualitative insight into the nature of vertical structures by considering the

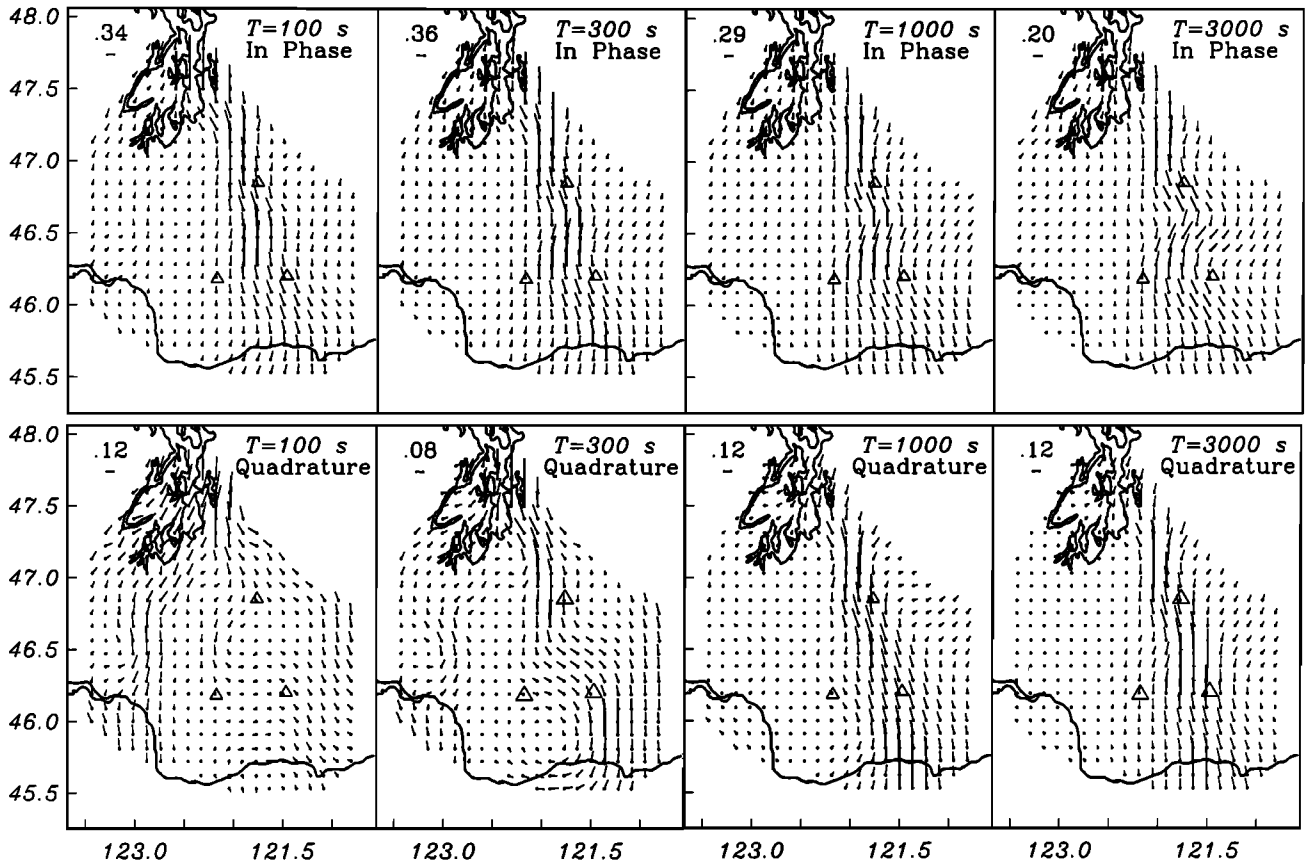

Fig. 10. Total current sheets as in Figure 9 for east-west source polarization. Here, at $T = 3000$ s, $\mathbf{I}_0 = .16\hat{\mathbf{x}}$ for in phase currents and $\mathbf{I}_0 = .08\hat{\mathbf{x}}$ for quadrature currents. Total currents for other periods are proportional to relative RMS as in Figure 9. Normal current flowing from the south is concentrated in the north-south trending SWCC. A smaller anomaly is visible in the western part of the array, particularly in the short-period quadrature plots.

period dependence and phase of the sheet currents in Figures 9 and 10.

The in-phase currents, which are larger than the corresponding quadrature currents by as much as a factor of 4, reveal the major structures most clearly. These are, to a first approximation, independent of period. The most obvious anomaly is the north-south trending SWCC mapped by *Stanley* [1984] and *Stanley et al.* [1987] using MT. This anomaly results in a substantial enhancement of currents under the Cascades for both polarizations but is clearest for east-west sources which excite current flow from south to north (Figure 10). The anomaly is widest and most diffuse in southern Washington near the Columbia river. North of Mount St. Helens and Mount Adams, the anomalous currents become more concentrated, and the estimated conductance increases steeply. Further north, near Mount Rainier, there is a kink in the anomalous currents where the conductor shown in Plate 1 narrows sharply. The anomalous currents then turn toward Puget Sound and become more diffuse again just south of Seattle.

The SWCC is also clearly evident in anomalous field plots for the north-south source polarization (which induces normal current flow from west to east). Current flowing from the east is channeled into the SWCC south of Mount Adams, with current flow across the eastern boundary of the SWCC severely reduced (Figure 9). To the west, current is concentrated in the CBC, which branches off of the SWCC just north of Mount St. Helens, and in a zone of enhanced conductivity beneath the Puget Lowlands northwest of Mount Rainier (Plate 1). Current flow along much of the western edge of the SWCC, which deflects and channels the currents north toward Puget Sound, is nearly north-south (Figure 9). This suggests a sharp transition to generally very resistive crust west of the SWCC. Here, the outcropping Crescent Formation basalts of the Willapa Hills in the southwestern part of the array and of the Black Hills to the north mark resistive blocks which are separated by a conductive channel beneath the northern edge of the Chehallis Basin. Note that the resistive block north of the CBC extends east to the SWCC beneath the sediments of the Puget Lowlands (Figure 9, Plate 1). Farther to the north, current flows west across Puget Sound and is deflected to the south along the eastern edge of Hood Canal by a resistive structure, which probably represents underthrust volcanics of the Crescent Formation on the eastern edge of the Olympic Peninsula.

At periods beyond 1000 s the anomalous currents have a fixed morphology with period-dependent but spatially constant amplitudes and phases (Figures 9 and 10). This is consistent with normal currents induced in a larger region, which are then distorted and channeled by local variations of conductivity in a thin surface layer [*Banks*, 1979; *Le Mouel and Menvielle*, 1982]. The spatially constant amplitudes and phases are determined by the normal fields, which depend on the large-scale deep regional conductivity structure, while the morphology of the anomalous fields is determined by local variations in crustal conductance. This supports the validity (for long periods) of the simple thin sheet model used to invert for crustal conductance. It also suggests that phases and relative amplitudes of regionally averaged electric fields can be approximately determined from the anomalous magnetic fields. At periods of the order 1000 s we would expect crustal electric currents in this region to be strongly influenced by currents (of large amplitude and low phase) induced in the highly conducting

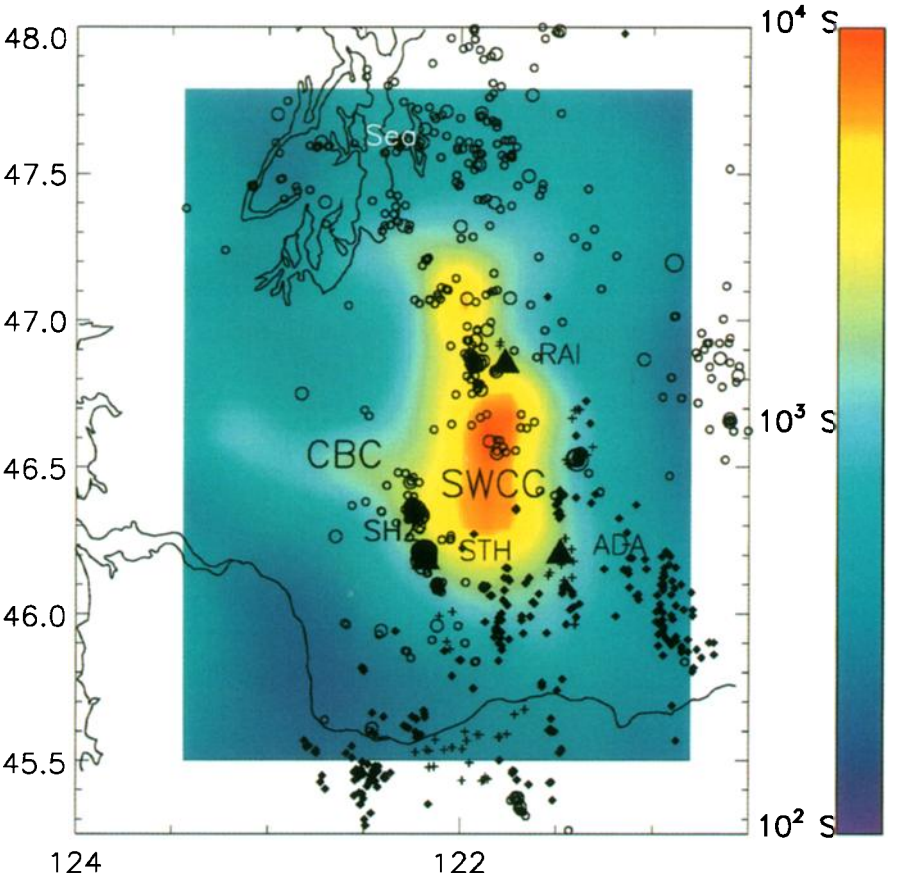

Plate 1. Thin sheet conductance model for the crust in southwestern Washington with crustal earthquakes and volcanic vents overlain. Earthquakes (0 to 15 km depth) are plotted as hexagons scaled by size (smallest, 2.0-3.9; medium, 4.0-4.9; large, 5.0-5.9). Small crosses are basaltic vents; small diamonds are andesite and dacite vents. The St. Helens Seismic zone (SHZ) coincides with the western edge of the broad southern portion of the SWCC, and is abruptly terminated by the east-west trending CBC. Volcanic vents cluster around the edges of the SWCC. Sea., Seattle; STH, Mount St. Helens; RAI, Mount Rainier; ADA, Mount Adams.

ocean [e.g., *Mackie et al.*, 1988]. In fact, for the north-south source polarization (Figure 9), for which oceanic effects should be strongest, phases of the long-period anomalous fields are very low ($\approx 10^\circ - 20^\circ$), and amplitudes remain large even at long periods. These characteristic oceanic effects are less prominent for east-west sources (Figure 10), for which phases are $\approx 25^\circ - 35^\circ$ and amplitudes decrease rapidly at long periods.

Although the full three-dimensional electromagnetic induction problem is complex and allows a great range of phenomena, the relative magnitudes of the in-phase and quadrature components of the anomalous fields provide a qualitative indication of the depths and sizes of conductive structures [e.g., *Schmucker*, 1970]. The phase of currents flowing in near-surface conductors is approximately the same as the phase of the surface electric fields (45° over a uniform conductor), so superficial conductivity anomalies tend to have large quadrature parts. Anomalous fields arising from currents flowing in conductors at greater depths (i.e., a significant fraction of the electromagnetic skin depth or more) tend to have small (or even negative) quadrature parts. Of course, whether a conductor is "near surface" or not depends on period. At long enough periods, all anomalies will appear near surface.

These points are nicely illustrated by Figure 10. In addition to the SWCC, a small north-south trending anomaly is visible in the western part of the array at $T = 100$ s but is almost unnoticeable at $T = 1000$ s. This feature is much stronger in the corresponding quadrature component, where this anomaly dominates at $T = 100$ s and is very clear for $T = 300$ s, before vanishing for longer periods. In fact, adjusting for differences in plot scales, we see that the in-phase and quadrature parts are roughly equal for $T = 100$ s, suggesting a shallow origin for this anomaly. This conclusion is supported by the rapid decrease of the anomaly with period. Comparison with Figure 1 shows that the anomaly coincides with the alignment of the Chehallis Basin and the western part of the Puget Lowlands. These basins contain conductive sediments and have a narrow connection south of Puget Sound. The magnitude, phase, and strong period dependence of these anomalous currents imply that the basins are distinct, with only a weak electrical connection.

By comparison, the anomalous fields over the SWCC in Figure 10 decrease in amplitude much more slowly (peaking near $T = 300$ s) and do not show consistently positive phases until $T = 1000$ s. The quadrature currents are restricted to the extreme northern part of the the anomaly at $T = 100$ s and extend further to the south with increasing period, until at $T = 1000$ s the plots closely resemble those for the in-phase currents. This suggests that the conductive rocks which form the SWCC are shallower in the north and deeper to the south. However, it is also possible that self-induction within the SWCC together with inductive and conductive coupling to Puget Sound in the north and the lower crustal conductor under the Oregon Cascades to the south [*Gough et al.*,

1989; *Wannamaker et al.*, 1989] can explain the period-dependent morphology of the quadrature anomalous currents. Three-dimensional modeling will ultimately be required for a full understanding of these data, although these results clearly demonstrate that the SWCC represents a conductor which is much more massive than a few kilometers of sediments. Note also that the in-phase currents flowing in the SWCC have a kink where the CBC branches off. The amplitude of this kink increases with period, and the kink is less obvious in the quadrature currents, suggesting a deep origin for this feature.

For the north-south polarization the quadrature currents closely resemble the in-phase parts at longer periods but not for $T = 100$–300 s (Figure 9). In these short-period quadrature plots, currents are large in the north, south, and east, but almost vanish in the west central part of the array, where the anomaly associated with the CBC fades out (compare to the in-phase parts). This large-scale variation of quadrature amplitudes suggests that phases in the electric fields are low in the region between the SWCC and the ocean. We note that *Stanley*'s [1984] MT results show very low electric field phases around 100 s periods in this area. Again, this behavior indicates complex three-dimensional inductive phenomena, here involving the interaction of the SWCC and the highly conducting ocean to the west.

The anomalous currents exhibit some more subtle but systematic variations with period. These are best explored by considering selected cross sections which allow results for all four periods to be superimposed. For this purpose we use the real parts of the scaled fields plotted in Figures 9 and 10. This effectively eliminates variations of normal field amplitudes and phases (largely determined by regional-scale induction effects), so that we may more directly assess changes with period of current morphology (which is more indicative of local structure). The conclusions we reach from these profiles are qualitative. More detailed mapping of vertical structure in conductivity variations suggested by this analysis requires MT data.

We consider two east-west profiles (Figure 8), A-A' across the northern part of the SWCC near Puget Sound and B-B' across the central portion of the SWCC. On the northern profile the relative amplitude of the anomaly decreases steadily with period, and the western boundary shifts slightly to the east (Figure 11*a*). On the central profile B-B', the anomaly peaks at 300 seconds. As period increases, the western limit of the anomaly shifts to the east, and a broad elevated shoulder on the anomaly develops to the east (Figure 11*b*). The shift of the anomaly peak suggests that the SWCC dips down to the east, while the broad spread to the east of anomalous currents at long periods suggests a deep conductive zone in the lower crust beneath the Columbia Plateau east of the Cascades.

Another view of the western boundary of the SWCC is given in Figure 11*c*, where we plot the currents which are induced by north-south sources and then channeled to the north across profile B-B'. Here the peak of the anomalous currents, which is fixed slightly to the west of the peak for east-west sources, steadily increases in amplitude with period. For a north-south polarization, current flows from the east and concentrates near the western boundary of the SWCC. The fixed location of the peak suggests a vertical western boundary. The increase in relative amplitude of the deflected currents suggests that a strong gradient in conductivity between the SWCC and the crust to the west persists at depth. Together the current profiles of Figures 11*b* and 11*c* suggest that the SWCC dips to the east but has a sharp, nearly vertical western boundary.

In Figure 12 we plot currents for the two north-south profiles,

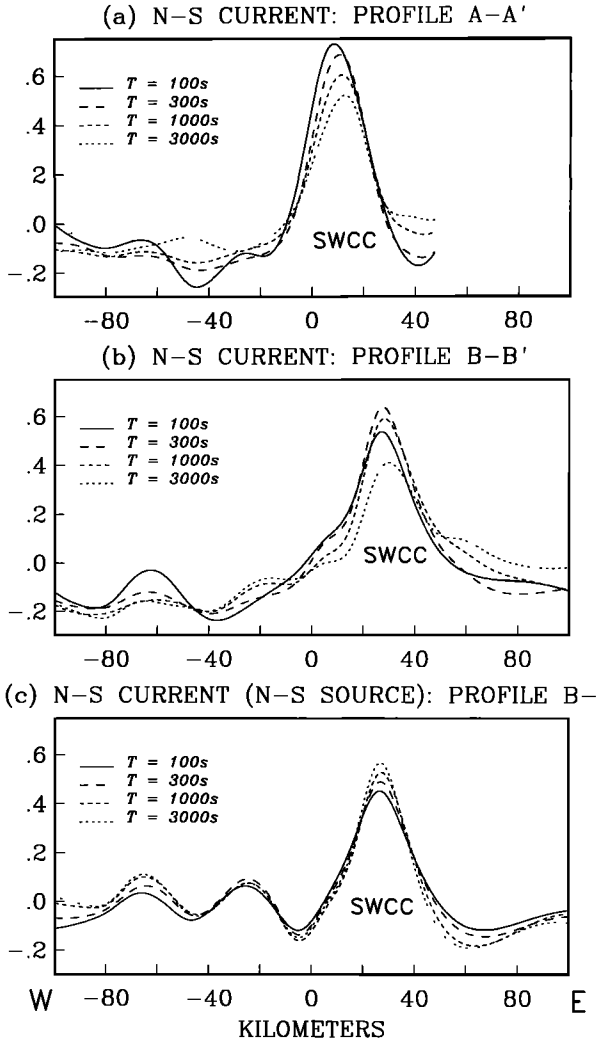

Fig. 11. Cross sections of crustal current flow derived from Figures 9 and 10 for two east-west profiles across the array (see Figure 8 for profile locations). (*a*) Relative anomalous current flow to the north across profile A-A' induced by east-west sources decreases at longer periods. (*b*) Further south on profile B-B' across the SWCC current shifts to the east at longer periods. (*c*) Channeled currents flow north across B-B' for north-south source polarization, which induces east-west normal currents. The relative amplitude increases steadily with period, but the location of the peak remains fixed, slightly to the west of the anomaly peak in Figure 11f1b.

C-C' and D-D' (Figure 8). For profile C-C' on the western edge of the SWCC, the peak associated with the CBC broadens and a second peak develops to the north as periods increase. Note that at $T = 3000$ s the secondary peak is well to the north of the Chehallis Basin, demonstrating that most of the current in the CBC does not flow out of the SWCC through the near-surface basin sediments. Further to the west on profile D-D', current flow is much more sharply peaked, centered along the northern edge of the Chehallis Basin. In both north-south profiles the second zone of enhanced current flow, across the northern part of the Puget Lowlands and through Puget Sound, is independent of period.

DISCUSSION

The MV array results are generally consistent with the conductivity models of *Stanley* [1984] and *Stanley et al.* [1987, 1990] based on three MT transects across southwestern Washington. In particular, the MV conductance model (Plate 1) is remarkably similar to the estimate of conductance for the SWCC given by

Stanley et al. [1987] (see Figure 1). However, the results given here provide a three-dimensional context in which to interpret the MT transects and suggest some differences. The two-dimensional model for the central MT profile (A-A' [*Stanley et al.*, 1987]) has a gradual boundary, with conductive sedimentary rocks thinning and shallowing to the west. However, the MT transect on which this model is based crosses the SWCC just north of Mount St. Helens where the CBC branches off. The MV data show that the western end of this transect is not typical of the SWCC; along most of the western edge, there is an abrupt and nearly vertical contact between very conductive and very resistive rocks (as seen also in the model for the northern MT profile C-C' of *Stanley et al* [1987]).

Stanley et al. [1987] model the SWCC dipping down to the east and suggest that the conductive unit has been underthrust and possibly continues to the east of the Cascades under the Columbia Plateau. The MV data, which show the anomalous magnetic fields shifting and broadening to the east at long periods, corroborate this. In the MT model the SWCC is bounded on the east by a resistive block which was interpreted by Stanley et al. to be a localized pluton. However, the MV results show east-west flowing currents channeled into the southern end of the SWCC by an elongated resistive block along its eastern boundary (Figure 9). This suggests that the resistive structure imaged on the MT transect is part of a deep, north trending resistive block which continues for 50-60 km and defines the eastern edge of the SWCC. The second MT profile (C-C') of Stanley et al., which crosses the SWCC just south of Puget Sound, shows the conductive zone narrowing, shifting to the west, and shallowing. All of these features are consistent with the pattern of anomalous currents and the model for crustal conductance of Plate 1.

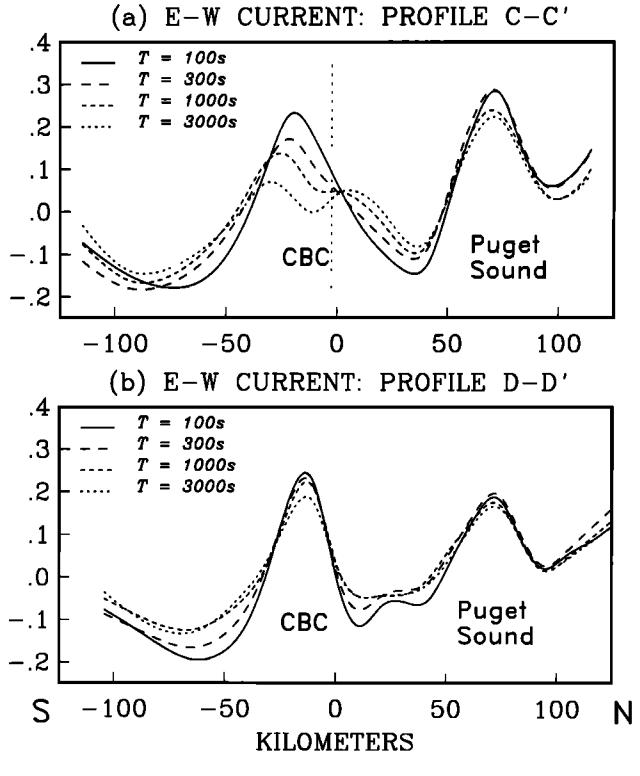

Fig. 12. East-west current flowing across profiles (*a*) C-C' and (*b*) D-D' (see Figure 8 for profile locations). In Figure 12fla current flowing to the west out of the SWCC shifts to the north at longer periods. The northern limit of the exposed sediments of the Chehallis Basin is indicated by the vertical dashed line. On the western profile in Figure 12flb, current morphology is relatively independent of period.

The variations of conductance inferred from the MV data correlate with and illuminate other geophysical constraints. In Plate 2 we superpose the estimated crustal currents induced by north-south polarized magnetic fields on a map of isostatic residual gravity [*Simpson et al.*, 1986; *Finn et al.*, 1986; *Williams et al.*, 1988]. The correlation of the sheet current and the gravity anomalies in the western part of the array is quite striking. The electric currents tend to flow around the gravity highs, which are strongly correlated with the resistive sections of the Coast Range block (compare to Plate 1). Note also the elongated weak high in the gravity map along the eastern boundary of the SWCC. The currents flow around this elongated resistive feature to enter the SWCC from the south.

The MV results are also consistent with major features in magnetic anomaly maps. As discussed by *Stanley et al.* [1987], the SWCC coincides with a substantial low in the magnetic data beneath the Cascades. The Coast Range block is characterized by a series of broad magnetic highs bounded on the east by a north-south trending line which likely extends south through Oregon [*Finn*, 1990; *Johnson et al.*, 1990]. *Finn* [1990] has pointed out that this boundary coincides closely with the western edge of the SWCC. Joint interpretation of gravity and magnetic data suggests a thick (20-30 km) section of dense highly magnetized rocks in the Coast Range block which *Finn* [1990] interprets as consisting of oceanic basalt and gabbro. In general, the very resistive sections of the Coast Range block (Plate 2) correspond with highs in the magnetic data, while the CBC corresponds to an east-west trending low [see *Finn*, 1990; Plate 2]. Note however that the magnetic high in the resistive block north of the CBC extends into the Chehallis Basin (well to the south of the gravity high seen in Plate 2). This suggests [*Finn*, 1990] that the northern edge of the Chehallis Basin is underlain (at shallow depths) by a thin lip of Coast Range mafic rocks, which have been underthrust by sediments along a northwest trending fault. This inference is strongly supported by our analysis of the MV array data.

Stanley et al. [1987, 1990] have noted that the spatial distribution of crustal seismicity in southwestern Washington appears to be closely related to the SWCC. A compilation of shallow (0-15 km) earthquake epicenters (C. Weaver and R. Ludwin, personal communication, 1992) shows a striking correlation with the MV crustal conductance model (Plate 1) and the equivalent sheet currents (Figure 13). The lower line of concentrated upper crustal seismicity (the SHZ [*Weaver and Smith*, 1984; *Weaver et al.*, 1987]) lies along the eastern boundary of the SWCC. The SHZ is truncated abruptly by the CBC. North of the CBC, the seismically active zone jumps to the east and deepens [*Ludwin et al.*, 1991]. Near Mount Rainier the earthquake epicenters are aligned with the narrow northern portion of the SWCC, and the seismically quiet zone west of Mount Rainier and south of Puget Sound coincides with the resistive block just to the west. The smaller east-west conductivity anomaly across southern Puget Sound marks the boundary between this quiet zone and the region of high seismic activity in the crust to the north.

In Plate 1 we have also plotted late Cenozoic (5 Ma and younger) volcanic vents [*Guffanti and Weaver*, 1988]. In southwestern Washington, these tend to cluster around the southern and eastern edges of the SWCC. In the same area along the southeastern edge of the conductivity anomaly, heat flow peaks at 80-90 mW m^{-2}, the highest value reached in the Washington Cascades [*Blackwell et al.*, 1990].

It is hard to avoid the conclusion that the SWCC represents a major structural feature in the crust of southwestern Washington which is to some extent controlling patterns of crustal deformation

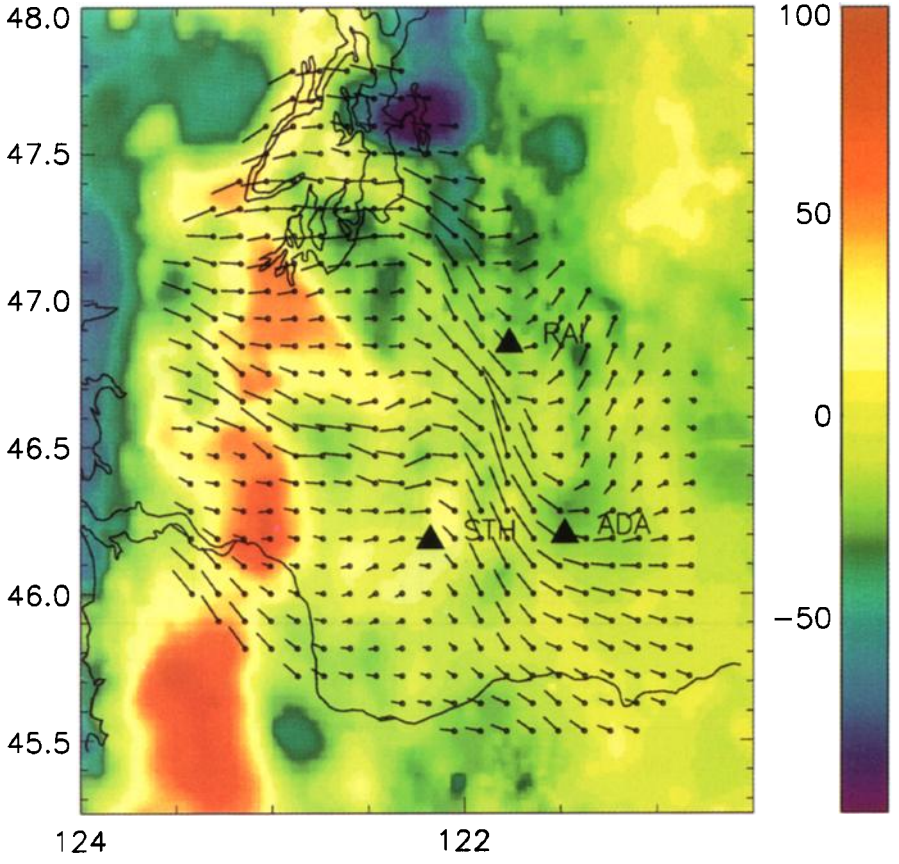

Plate 2. Isostatic residual gravity in western Washington with equivalent sheet current overlain. Reds are gravity highs; greens and blues are gravity lows. The scale on the right is in milligals. The pattern of current flow in the western part of the study area is consistent with channeling of currents around the "islands" of resistive and dense Crescent Formation mafic rocks. Note also the weak elongated gravity high on the eastern edge of the SWCC. Currents form the east flow around this feature to enter the SWCC from the south. STH, Mount St. Helens; RAI, Mount Rainier; ADA, Mount Adams.

and volcanism. Earthquakes and volcanic vents concentrate on the boundary of the anomaly but are almost absent in the interior. The SWCC thus represents a distinct block of crust which is bounded by narrow zones of active deformation. The deformation zones contain regions of local crustal extension conducive to the formation of volcanic vents [*Weaver et al.*, 1987]. The chain of late Cenozoic volcanic vents on the eastern boundary of the SWCC may reflect more active deformation along this boundary in the recent past. The lack of earthquakes and volcanic vents in the interior of the SWCC and the geometry of the conductor (localized in space, extending from near the surface to great depths) together argue against some possible explanations for the SWCC, such as a magma body under the Cascades or highly fractured rocks filled with hot saline water. The location of the peak heat flow on the boundary rather than in the interior of the SWCC reinforces this conclusion.

The MV results strongly support the conclusions of *Stanley et al.* [1987, 1990] concerning the geometry and conductivity of the SWCC. There is a massive unit of very conductive rocks under the Cascades which narrows to the north and probably dips down to the east. The high conductivity is most likely intrinsic to the rocks rather than being caused by current conditions in the crust such as the presence of hydrothermal fluids or magma. *Stanley et al.* [1987, 1990] considered a range of possible lithologies for these conductive rocks and concluded that at least the deeper part of the SWCC is most probably dominated by shale facies. Shales hold water trapped in clays and zeolites and can remain highly conductive even at the low porosities which should prevail at depths greater than a few kilometers.

Stanley et al. [1987] conclude that the SWCC is formed from accretionary prism and forearc basin marine sedimentary rocks which were trapped and compressed against the pre-Tertiary margin of North America when the Crescent basalts were accreted in the Eocene. This is an attractive hypothesis, but it raises some other questions. The SWCC is unique in Washington and Oregon, as evidenced by the EMSLAB MV array, which covered both states completely [*Gough et al.*, 1989]. Although smaller local induction anomalies associated with the suture zone between the Coast Range block and older Tertiary rocks to the east cannot be ruled out, the accumulation of the large volumes of conductive sediment seen in the SWCC is clearly unique to southwestern Washington.

The SWCC is an important structure which models for the tectonic history of the region must explain. What is special about this small section of the Coast Range suture zone? One possible suggestion is that the SWCC represents a section of the early Cenozoic subduction zone which is analogous to the present day Olympic Peninsula, where an anomalously thick section of sediments is being scraped off of the downgoing slab and piled up on the edge of the continent at a highly localized bend in the modern subduction zone. In this model, the sediments that make up the SWCC could have been accreted well before the Crescent basalts

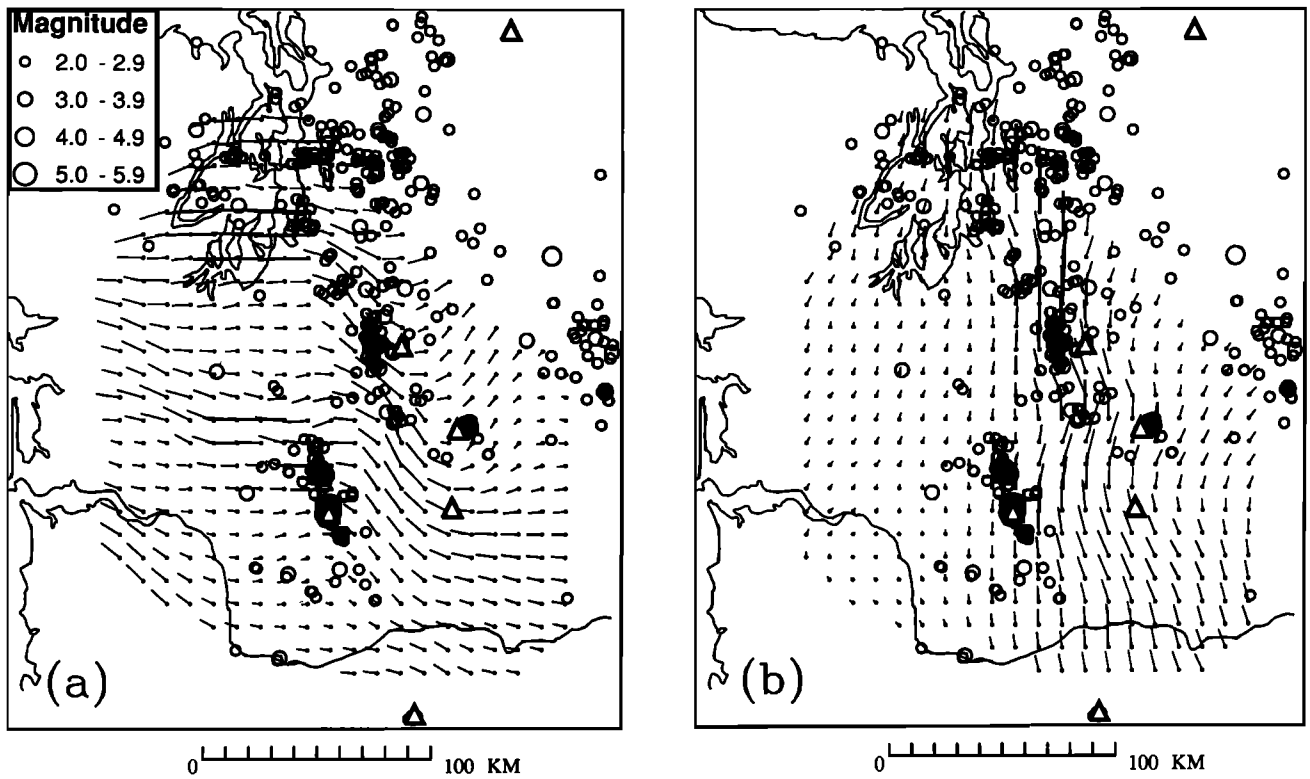

Fig. 13. Seismicity of western Washington (0-15 km) plotted on top of anomalous sheet electric currents observed by an MV array. Symbols are sized by magnitude: smallest, 2.0-3.9; medium, 4.0-4.9; largest, 5.0-5.9. The large triangles are the locations of the major Cascade volcanos. (*a*) The source polarization would drive the electric currents east-west in the absence of anomalous structure. Note how the currents entering in the southeast are deflected north as they run up against the seismic lineation of the SHZ. The SHZ is a boundary between a very resistive block to the west and the SWCC to the east. Note also how the currents are deflected around the very resistive and nearly aseismic block west of Mount Rainier, north of the SHZ and south of Puget Sound. Finally, note how the currents in the western Puget Sound region are deflected to the southwest, presumably by the resistive Coast Range block. (*b*) The source polarization would drive the electric currents north-south in the absence of anomalous structure. Note the very strong current in the SWCC between the SHZ and Mount Adams. This strong current continues well north of Mount Rainier.

were erupted. *Brandon and Calderwood* [1990] have suggested that the location of the Olympic subduction complex is controlled by the upwarping of the Juan de Fuca plate required to accommodate the reversed arc of the subduction zone resulting from Basin and Range extension. Thus the presence of an earlier zone of similar scale and probable composition places constraints on the geometry of the early Cenozoic subduction zone.

The MV data also image significant structure in the Coast Range rocks west of the SWCC. Here the crust is resistive over a very thick section, with two narrow east-west zones of relatively high conductivity. The clearest of these structures is the CBC, which lies on the northern edge of the Chehallis Basin. Currents flowing in near-surface basin sediments cannot explain the amplitude or period dependence of this anomaly. For east-west source polarizations there is a small north-south trending anomaly aligned with the exposed sediments of the Chehallis Basin and Puget Lowlands, but this vanishes for periods beyond 300 seconds. The much stronger, nearly period-independent east-west trending anomaly associated with the CBC clearly indicates a much deeper structure. Near the western boundary of the SWCC, the CBC appears to extend beneath resistive crust to the north. The crustal blocks to either side of the CBC are highly resistive throughout, from the SWCC to the outcropping Crescent Formation basalts (the Black and Doty Hills for the northern block and the Willapa Hills for the southern block). The northern edge of the Chehallis Basin is marked by numerous thrust faults (generally downthrown to the south [*Walsh et al.*, 1987]). To the north lies a series of west-northwest trending anticlines. We interpret the CBC as a section of conductive marine sedimentary rocks which have been thrust under the resistive accreted oceanic basement rocks to the north. *Wells and Coe* [1985] present a model for Eocene tectonics of southwestern Washington in which the oceanic "Crescent" plate was folded and broken into smaller blocks, which were subsequently thrust together during accretion to the continent. It is quite possible that the CBC resulted from this process and is thus a fundamental structural boundary in the Coast Range rocks.

The second zone of enhanced conductivity in the Coast Range block branches off of the top of SWCC, trends west across the northern portion of the Puget Lowlands, and is then deflected to the south by the crescent basalts on the eastern edge of the Olympic Peninsula (Plate 1, Figure 9). This structure is similar to the CBC in that it represents a deep conductive zone which separates resistive crustal blocks marked by exposed sections of the Crescent basalts (in this case the eastern Olympic Peninsula and the Black Hills). There is also some suggestion in Figure 9 (which is supported by the much larger scale EMSLAB array; see *Gough et al* [1989]) of an additional east-west conductive channel just off the bottom of the array coverage south of the Willapa Hills. It is tempting to suggest that these features are analogous to the CBC, and represent zones of sediments which were thrust beneath discrete blocks of resistive oceanic crust during accretion. How-

ever, the geometry of these conductive zones is poorly constrained by existing array coverage.

The large clockwise rotation of the accreted terranes of southwestern Washington since the Eocene have been attributed to tectonic processes operating at two distinct scales [*Wells*, 1990]. Dextral shear rotation of the continental margin driven by oblique subduction of the Juan de Fuca plate [*Beck*, 1980; *Wells et al.*, 1984] is accomplished through relative motions of a large number of elongated but thin (5-20 km) slices of crust. From the pattern of surface faulting and the geographic distribution of paleomagnetic rotations, *Wells and Coe* [1985] and *Wells* [1990] argue that this represents the dominant mode of postaccretion deformation in southwestern Washington. Late Cenozoic rotation at a larger scale has been attributed to motion of a rigid microplate in front of Basin and Range extension [*Simpson and Cox*, 1977; *Magill et al.*, 1981, 1982]. This mechanism probably dominates in the coast range of Oregon and likely also plays a role in crustal deformation and rotation in southwestern Washington, which occupies a transition zone between compressional and extensional tectonic regimes to the north and south, respectively [*Guffanti and Weaver*, 1988; *Wells*, 1990]. The crustal structures imaged by the MV data represent an intermediate scale. These structures appear to exert considerable control over the tectonics of this region. As discussed above, patterns of current seismicity and recent volcanism are strongly correlated with the MV conductance model. In addition, the grain of fault patterns appears to be correlated with the structures imaged by the MV data. *Wells and Coe* [1985] show left-lateral faults associated with shearing and rotation to trend west-northwest in the Willapa Hills block but east-northeast in the Black Hills block to the north. These observations suggest that the deep conductive structures imaged by the MV data represent soft zones which to some degree mechanically decouple the more rigid intervening resistive blocks. Thus, although large-scale gradients in the pattern of seismicity, volcanism, and crustal deformation and rotation in the Pacific Northwest are controlled by regional tectonics, the detailed distribution of these features on intermediate scales is also significantly affected by existing structures in the complex accreted crust.

A clearer image of the vertical profile of conductivity through the crust in this region would be highly desirable. Although full three-dimensional inversion of the MV array data would be a useful step in this direction, the intrinsic vertical resolution of MV data is low. Significant improvements in vertical resolution will require MT data. However, success with MT requires detailed mapping with closely spaced electric field measurements, which in practice requires data to be collected on a limited number of two-dimensional transects. On the other hand, MV data can be collected at relatively low cost using small (5-10 station) sequential overlapping arrays and then merged into synthetic arrays. MV array data thus represent an economical way to map major crustal conductivity variations (with poor vertical resolution) over a large area. Even with a wide station spacing, MV data can be useful for reconnaissance before more detailed MV or MT experiments are conducted. The MV and MT methods are thus complementary and should probably be used together in areas where three-dimensional complications are likely. By itself, MV array data can provide substantial insight into crustal structure. If used in conjunction with MT and other data, the potential of this geophysical tool is even greater. Indeed, joint inversion of MT profiles and MV array data probably offers the best practical hope for constructing three-dimensional images of crustal conductivity variations.

APPENDIX: EQUIVALENT SHEET CURRENTS AND THIN SHEET CONDUCTANCE

Here we discuss a refinement of the equivalent current transform and summarize our inversion of smooth anomalous field data for crustal conductance. We consider the simple thin sheet model of *Price* [1949], which consists of a thin conductive surface sheet of variable conductance

$$S(x, y) = S_0 + \delta S(x, y)$$

over a layered one-dimensional Earth which is separated from the surface sheet by a layer of infinite resistance.

Because of the resistive layer the current in the surface layer $\mathbf{I}(x,y) = \mathbf{I}_0 + \delta\mathbf{I}(x,y)$ satisfies $\nabla\cdot\mathbf{I} = 0$ and thus may be expressed in terms of a stream function

$$I_x(\mathbf{x}) = \frac{\partial\psi(\mathbf{x})}{\partial y} \qquad I_y(\mathbf{x}) = -\frac{\partial\psi(\mathbf{x})}{\partial x}. \tag{A1}$$

In the wavenumber domain, $\tilde{\psi}$ can be related to the anomalous magnetic field components $\tilde{H}_x$ and $\tilde{H}_z$ [*Berdichevsky and Zhdanov*, 1984]

$$\tilde{\psi}(k_x, k_y) = \frac{i}{\eta^2}\left[\eta^2\frac{\tilde{H}_x(k_x,k_y)}{k_x} + \omega\mu_0\tilde{H}_z(k_x, k_y)(S_0 - 1/Z_\eta)\right] \tag{A2}$$

where the tilde denotes the spatial Fourier transform, k_x and k_y are the horizontal wavenumbers, $\eta^2 = k_x^2 + k_y^2$, and Z_η is the wavenumber-dependent impedance for the normal one-dimensional conductivity section. Thus for this simple thin-sheet model the impedance of the underlying one-dimensional Earth can be used to exactly transform the anomalous magnetic fields into the anomalous current flowing in the surface layer. Note that in the limit $\omega \to 0$, the transformation reduces to rotating the anomalous field vectors 90° counterclockwise. Equations (A1) and (A2) represent a refinement of the simple transformation of section 3 to take account of the field produced on the surface by image currents induced in the underlying one-dimensional section by the anomalous currents in the sheet. Note that it is implicit in (A2) that constant (zero wavenumber) sheet currents cannot be uniquely determined from the anomalous fields (for which the zero wavenumber component is also ambiguous).

In fact, knowing the anomalous surface current for two orthogonal source polarizations is nearly enough to determine the conductance of the surface layer for this simple model. Let $R(x, y) = R_0 + \delta R(x, y) = 1/S(x, y)$ be the surface resistance. Then, since $\mathbf{E}(x, y) = R(x, y)\mathbf{I}(x, y)$, we have from Faraday's law

$$\frac{\partial}{\partial x}(R(x, y)I_y(x, y)x - \frac{\partial}{\partial y}(R(x, y)I_x(x, y)) = i\omega\mu H_z(x, y). \tag{A3}$$

Equation (A3) must be satisfied for currents induced by sources of both orthogonal polarizations for all frequencies for which the thin sheet approximation is valid. An analysis of the uniqueness of the resistance satisfying (A3) shows that if $\omega \neq 0$ and $\mathbf{I}$ is known for two orthogonal source polarizations (more precisely, for two current distributions which are parallel only on a set of measure zero), then R is uniquely determined. For $\omega = 0$, the resistance is determined only up to a scalar multiple. Unfortunately, the thin sheet approximation is most reasonable as $\omega \to 0$, so that in practice, the absolute scale of the crustal resistance cannot be determined from anomalous field data alone. The average

resistance R_0, or some equivalent reference, must be specified. Furthermore, the anomalous magnetic fields, which we can estimate, determine only the anomalous currents $\delta\mathbf{I}(x, y)$. The uniform part of the current flowing in the sheet, $\mathbf{I}_0$, is not determined from surface observations of the magnetic fields (or from (A1) and (A2)), but is needed to invert the anomalous current for surface conductance.

$\mathbf{I}_0$ is not completely arbitrary. For instance, setting $\mathbf{I}_0 = 0$ yields the equivalent currents plotted in Figure 8. This figure shows a number of unphysical current vortices. Indeed, in the low-frequency limit (probably a good approximation at 1000 seconds), the right-hand side of (A3) vanishes, and we must have for any closed contour C in the plane

$$\oint_C d\mathbf{l}\cdot\mathbf{I}(x, y)R(x, y) = 0 . \qquad \text{(A4)}$$

Since $R(x, y) > 0$, closed circulations of the currents are impossible. By adding a sufficiently large $\mathbf{I}_0$ to the anomalous fields, these current vortices disappear (Figures 9 and 10). (A4) thus provides a means to determine an approximate lower bound on $\mathbf{I}_0$. This can be implemented more directly by leaving $\mathbf{I}_0$ as a free parameter in the inversion. For total current vectors which are too small, the fit will be poor. By leaving $\mathbf{I}_0$ free to vary, misfits can be improved. Note, however, that as $\mathbf{I}_0$ gets very large, only small variations in surface conductance will be required to fit the anomalous field data, so the size of the total current must be controlled. In fact, the magnitude of the total magnetic fields observed on the surface of the Earth also imposes an upper bound on the magnitude of $\mathbf{I}_0$. Knowledge of a "normal" conductivity section, including information about large-scale lateral heterogeneities, could be used to refine bounds on current flow in the surface layer.

Given $\mathbf{I}_0$, R_0, the normal one-dimensional impedance, and an estimate of the anomalous horizontal magnetic fields, we can seek $\delta R(x, y)$. Equation (A3) can be expressed in the wavenumber domain as

$$\eta^2 R_0 \tilde{\psi}(k_x, k_y) - i\omega\mu_0 \tilde{H}_z(k_x, k_y) - i[k_x I_{0x} - k_y I_{0y}]\tilde{\rho}(k_x, k_y) - \frac{1}{4\pi^2}\iint d\alpha d\beta \psi(k_x-\alpha, k_y-\beta)(k_x(k_x-\alpha)+k_y(k_y-\beta))\tilde{\rho}(k_x, k_y) = 0 . \qquad \text{(A5)}$$

This integral equation in the unknown $\tilde{\rho}(k_x, k_y)$ (the Fourier transform of $\delta R(x, y)$) must be satisfied for stream functions $\tilde{\psi}$ determined from both polarizations (and for all frequencies for which the thin sheet approximation is reasonable). Note also that $\tilde{\rho}$ must be the Fourier transform of a real function. As a consequence, (A5) approximated on a discrete grid represents an overdetermined linear system. Within the limits of this model, inversion for surface conductance can be accomplished as follows. The smooth spline estimates of the anomalous magnetic fields can be estimated on a regular grid, Fourier transformed, and, using (A2), used to estimate $\tilde{\psi}$. A discrete version of (A5) for a pair of source polarizations at one or more sufficiently long periods can then be inverted using damped least squares. The resulting estimate $\tilde{\rho}$ is then back transformed to yield the variation in resistance and ultimately the thin sheet conductance.

Acknowledgments. Assistance in data collection was provided by E.G. Hensel, J.T. Smith, and P. Russell. Support for parts of this work was provided by NSF grants EAR-8307681, EAR-8410638, EAR-8721091, EAR-9005207 and USGS grant 14-08-0001-20576.

REFERENCES

Armentrout, J.M., Cenozoic stratigraphy, unconformity-bounded sequences, and tectonic history of southwestern Washington, *Wash. Div. of Geol. Earth Res. Bull., 77*, 291-320, 1987.

Bailey, R.C., R.N. Edwards, G.D. Garland, R. Kurtz, and D. Pitcher, Electrical conductivity studies over a tectonically active area in eastern Canada, *J. Geomagn. Geoelectr., 26*, 125-146, 1974.

Banks, R.J., The use of equivalent current systems in the interpretation of geomagnetic depth sounding data, *Geophys. J. R.Asstron. Soc., 56*, 139-157, 1979.

Banks, R.J., The interpretation of the Northumberland Trough geomagnetic variation anomaly using two-dimensional current models, *Geophys. J. R. Astron. Soc., 87*, 595-616, 1986.

Banks, R.J., and D. Beamish, Local and regional induction in the British Isles, *Geophys. J. R. Astron. Soc., 79*, 539-553, 1984.

Beamish, D., The mapping of induced currents around the Kenya rift: A comparison of techniques, *Geophys. J. R. Astron. Soc., 50*, 311-332, 1977.

Beamish, D., and R.J. Banks, Geomagnetic variation anomalies in northern England: Processing and presentation of data from a non-simultaneous array, *Geophys. J. R. Astron. Soc., 75*, 513-539, 1983.

Beck, M.E., Jr., Paleomagnetic record of plate-margin tectonic processes along the western edge of North America, *J. Geophys. Res., 85*, 7115-7131, 1980.

Berdichevsky, M.N., and M.S. Zhdanov, *Advanced Theory of Deep Geomagnetic Sounding*, 408 pp., Elsevier, New York, 1984.

Blackwell, D.D., J.L Steele, and S. Kelley, Heat flow in the state of Washington and thermal conditions in the Cascade Range, *J. Geophys. Res., 95*, 19,495-19,516, 1990.

Booker, J.R., and E.G. Hensel, Delineation of the crustal path of a channeled current in the ocean, paper presented at the Sixth Workshop on Electromagnetic Induction in the Earth and Moon, Int. Assoc. of Geomagn. and Aeron., Victoria, B.C., 1982.

Brandon, M.T., and A.C. Calderwood, High-pressure metamorphism and uplift of the Olympic subduction complex, *Geology, 18*, 1252-1255, 1990.

Cady, W.M., Tectonic setting of the tertiary volcanic rocks of the Olympic Peninsula, Washington, *J. Res. U.S. Geol. Surv., 3*, 573-582, 1975.

Clowes, R.M., M.T. Brandon, A.G. Green, C.J. Yorath, A. Sutherland Brown, E.R. Kanesewitch, and C. Spencer, LITHOPROBE - Southern Vancouver Island: Cenozoic subduction complex imaged by deep seismic reflections, *Can. J. Earth Sci., 24*, 31-51, 1987.

Cowan, D.S., and C.J. Potter, Continental-oceanic transect B-3; Juan de Fuca plate to Montana Thrust Belt, *Cont. Oceanic Transect Ser.*, vol. 9, Geol. Soc. of Am., Boulder, Colo., 1986.

Duncan, R.A., A captured island chain in the coast range of Oregon and Washington, *J. Geophys. Res., 87*, 10,827-10,837, 1982.

Duncan, R.A., and L.D. Kulm, Plate tectonic evolution of the Cascades arc-subduction complex, in *The Geology of North America, The Eastern Pacific Ocean and Hawaii*, vol. N, edited by E.L. Winterer, D.M. Hussong, and R.W. Decker, pp. 413-438, Geological Society of America, Boulder Colorado, 1989.

Egbert, G.D., Multivariate splines for interpolation and separation of magnetometer array data, paper presented at Sixth Scientific Assembly, Int. Assoc. of Geomagn. and Aeron., Exeter, England, July 24 - Aug. 4, 1989.

Egbert, G.D., On the synthesis of a large geomagnetic array from small overlapping arrays, *Geophys. J. Int., 106*, 37-51, 1991.

Egbert, G.D., and J.R. Booker, Multivariate analysis of geomagnetic array data 1, The response space, *J. Geophys. Res., 94*, 14,227-14,248, 1989.

Everett, J.E., and R.D. Hyndman, Geomagnetic variations and electrical conductivity structure in south-western Australia, *Phys. Earth Planet. Inter., 1*, 24-34, 1967.

Fainberg, E.B., A.V. Kuvshinov, and B.S. Singer, Electromagnetic induction in a spherical earth with non-uniform oceans and continents in electric contact with the underlying medium, 1, Theory method and example, *Geophys. J. Int., 102*, 283-286, 1990.

Finn, C., Constraints on Washington convergent margin structure, *J. Geophys. Res., 95*, 19,533-19,546, 1990.

Finn, C., D.L. Williams, R.W. Couch, Z.F. Danes, G.S. Pitts, and W.M. Phillips, Gravity anomaly and terrain maps of the Cascade Range, California, Oregon, Washington, and British Columbia, scale 1:2,500,000, U.S. Geol. Surv. Geophys. Invest. Map GP-972, 2 sheets, 1986.

Gough, D.I., Magnetometer array studies, earth structure, and tectonic processes, *Rev. Geophys., 27*, 141-157, 1989.

Gough, D.I., D.M. McKirdy, D.V. Woods, and H. Geiger, Conductive

structures and tectonics beneath the EMSLAB land array, *J. Geophys. Res., 94*, 14,099-14,110, 1989.

Guffanti, M., and C.S. Weaver, Distribution of late Cenozoic volcanic vents in the Cascade Range: Volcanic arc segmentation and regional tectonic considerations, *J. Geophys. Res, 93*, 6513-6529, 1988.

Johnson, P.R., I. Zietz, and K.R. Bond, U.S. west coast revisited: An aeromagnetic perspective, *Geology, 18*, 332-335, 1990.

Law, L.K., D.R. Auld, and J.R. Booker, A geomagnetic variation anomaly coincident with the Cascade volcanic belt, *J. Geophys. Res., 85*, 5297-5302, 1980.

Le Mouel, J.L., and M. Menvielle, Geomagnetic variation anomalies and deflection of telluric currents, *Geophys. J. R. Astron. Soc., 68*, 575-587, 1982.

Ludwin, R.S., C.S. Weaver, and R.S. Crosson, Seismicity of Washington and Oregon, in *Neotectonics of North America*, edited by D.B. Slemmons, E.R. Engdahl, M.D. Zoback, and D.D. Blackwell, pp. 77-98 Geological Society of America, Boulder, Colo., 1991.

Mackie, R.L., B.R. Bennett, and T.R. Madden. Long period magnetotelluric measurements near the central California coast: A land-locked view of the conductivity structure under the Pacific Ocean, *Geophys. J., 95*, 181-194, 1988.

Magill, J., A. Cox, and R. Duncan, Tillamook volcanic series: Further evidence for tectonic rotation of the Oregon Coast Range, *J. Geophys. Res., 86*, 2953-2970, 1981.

Magill, J.R., R.E. Wells, R.W. Simpson and A.V. Cox, Post 12 m.y. rotation of southwest Washington, *J. Geophys. Res., 87*, 3761-3776, 1982.

Meingut, J., An intrinsic approach to multivariate spline interpolation at arbitrary points, in *Polynomial and Spline Approximation*, edited by B.N. Sahney, pp. 163-190, D. Reidel, Norwell, Mass., 1979.

Muffler, L.J.P., Introduction to special section on the geological, geophysical, and tectonic setting of the Cascade range, *J. Geophys. Res., 95*, 19,407-19,408, 1990.

Parker, R.L., and L. Shure, Efficient modeling of the Earth's magnetic field with harmonic splines. *Geophys. Res. Lett., 9*, 812-815, 1982.

Parkinson, W.D., The influence of continents and oceans on geomagnetic variations, *Geophys. J. R. Astron. Soc., 4*, 441-449, 1962.

Price, A.T., The induction of electric currents in non-uniform thin sheets and shells, *Q. J. Mech. Appl. Math., 2*, 283-310, 1949.

Rokityansky, I.I., *Geoelectromagnetic Investigation of the Earth's Crust and Mantle*, New York: Springer-Verlag, 381 pp, 1982.

Schmucker, U., Anomalies of geomagnetic variations in the southwestern United States, *Bull. Scripps Inst. Oceanogr., 13*, 1970.

Shure, L., R.L. Parker, and G.E. Backus. Harmonic splines for geomagnetic modeling. *Phys. Earth Planet. Inter. 28*, 215-229, 1982.

Simpson, R.W., and A.V. Cox, Paleomagnetic evidence for tectonic rotation of the Oregon Coast Range, *Geology, 5*, 585-589, 1977.

Simpson, R.W., R.C. Jachens, R.J. Blakely, and R.W. Saltus, A new isostatic residual gravity map of the conterminous United States with a discussion on the significance of isostatic residual anomalies, *J. Geophys. Res., 91*, 8348-8372, 1986.

Snavely, P.D., Jr., and H.C. Wagner, Geologic cross section across the continental margin of southwestern Washington, *U.S. Geol. Surv. Open File Rep. 82-459*, 10 pp., 1982.

Snavely, P.D., Jr., N.S. MacLeod, and H.C. Wagner, Tholeiitic and alkalic basalts of the Eocene Siletz River volcanics, Oregon Coast Range, *Am. J. Sci., 266*, 454-481, 1968.

Stanley, W.D., Tectonic study of Cascade Range and Columbia Plateau in Washington State based on magnetotelluric soundings, *J. Geophys. Res., 89*, 4447-4460, 1984.

Stanley, W.D., C. Finn, and J.L. Plesha, Tectonics and conductivity structures in the southern Washington Cascades, *J. Geophys. Res., 92*, 10,179-10,193, 1987.

Stanley, W.D., W.D. Mooney, and G.S. Fuis, Deep crustal structure of the Cascade Range and surrounding regions from seismic refraction and magnetotelluric data, *J. Geophys. Res., 95*, 19,419-19438, 1990.

Taber, J.J., and S.W. Smith, Seismicity and focal mechanisms associated with the subduction of the Juan de Fuca plate beneath the Olympic Peninsula, Washington:*Bull. Seismo. Soc. Am., 75*, 237-249, 1985.

Tabor, R.W., and W.M. Cady, The structure of the Olympic Mountains, Washington-Analysis of a subduction zone, *U.S. Geol. Surv. Prof. Pap.* 1033, 38 pp., 1978.

Trehu, A.M., J. Nabelek, S. Avezedo, T. Brocher, W. Mooney, J. Luetgert, I. Asudah, R. Clowes, Y. Nakamura, and K. Miller, A crustal cross-section across the Cascadia subduction zone in central Oregon, (abstract), *Eos Trans. AGU, 73(43)*, Fall Meeting suppl., 391, 1992.

Trigg, D.G., P.H. Serson, and P.A. Camfield, A solid state electrical recording magnetometer, *Publ. Earth Phys. Branch Can., 41*, 67-80, 1970.

Vasseur, G., and P. Weidelt, Bimodal electromagnetic induction in non-uniform thin sheets with an application to the northern Pyrenean induction anomaly, *Geophys. J. R. Astron. Soc., 51*, 669-690, 1977.

Wahba, A.M., and J. Wendelberger, Some new mathematical methods for variational objective analysis using splines and cross-validation, *Mon. Weather Rev., 108*, 1122-1143, 1980.

Walsh, T.J, M.A. Korosec, W.M. Phillips, R.L. Logan, and H.W. Schasse, Geology map of Washington - Southwest quadrant, *Geol. Map GM-34*, 28 pp., scale 1:250,000, Wash. Div. of Geol. and Earth Resour., Olympia, 1987.

Wannamaker, P.E., J.R. Booker, A.G. Jones, A.D. Chave, J.H. Filloux, H.S. Waff, and L.K. Law, Resistivity cross-section through the Juan de Fuca subduction system and its tectonic implications, *J. Geophys. Res., 94*, 14,127-14,145, 1989

Weaver, C.S., and S.W. Smith, Regional tectonic and earthquake hazard implications of a crustal fault zone in southwestern Washington, *J. Geophys. Res., 88*, 10,371-10,383, 1983.

Weaver, C.S., W.C. Grant, and J.E. Shemeta, Local crustal extension at Mount St. Helens, Washington, *J. Geophys. Res., 92*, 10,170-10,178, 1987.

Weaver, J.T., The electromagnetic field within a discontinuous conductor with reference to geomagnetic micropulsations near a coastline, *Can. J. Phys., 41*, 1962.

Wells, R.E., Paleomagnetic rotations and the Cenozoic tectonics of the Cascade arc, Washington, Oregon and California, *J. Geophys. Res., 95*, 19,409-19,417, 1990.

Wells, R.E., and R.S. Coe, Paleomagnetism and geology of Eocene volcanic rocks of southwestern Washington, Implications for mechanisms of rotation, *J. Geophys. Res., 90*, 1925-1947, 1985.

Wells, R.E., D.C. Engebretson, P.D. Snavely Jr., and R.S. Coe, Cenozoic plate motions and the volcanotectonic evolution of western Oregon and Washington, *Tectonics, 3*, 275-294, 1984.

Williams, D.L., C. Finn, R.W. Couuch, Z.F. Danes, G.S. Pitts, W.M. Phillips, and R.P. Riddihough, Residual Bouguer gravity anomaly map of the Cascade Range, California, Oregon, Washington, and British Columbia, *U.S. Geol. Surv. Geophys. Inv. Map GP-973*, 2 sheets, scale 1:500,000, 1988.

J. R. Booker, Geophysics Program AK-50, University of Washington, Seattle WA 98195.

G. D. Egbert, College of Oceanic and Atmospheric Sciences, Oregon State University, Oceanography Admin. Bldg. 104, Corvallis, OR, 97330-5503.

(Received July 10, 1992;
revised March 19, 1993;
accepted March 23, 1992.)